Bold application of sNDM to REA in a SSCR core with azimuthal mesh

Alexis Nuttin, Nicolas Capellan, Olivier Méplan

Bold application of sNDM to REA in a SSCR core with azimuthal mesh

A. Nuttin (nuttin@lpsc.in2p3.fr), N. Capellan, O. Méplan

Research Report LPSC-24-01 (February 2024)

ABSTRACT

Previously applied to REA (Rod Ejection Accident) in several PWR-like cores, the minimalistic Nodal Drift Method (NDM) has recently been generalized to sNDM (super NDM). Both developed and validated on a heat-up transient of the KRUSTY experiment made of a few homogeneous parts, sNDM basically feeds the one-group diffusion approximation with so-called corrective Surface Factors (SF) for internodal currents from MCNP F1 tallies. In order to specify its practical usefulness for exploratory design studies, sNDM at its turn is put to the demanding test of REA in a PWR-like core. The chosen test case is a 600 MW_{th} D_2O/H_2O-cooled thorium-fueled Spectral Shift Control Reactor (SSCR) core retrieved from previous studies, whose main results on conversion (by our MC-based tool SMURE) and safety (by NDM) are first summed up. Enhanced MCNP core models at HFP, CZP and HZP (respectively Hot Full, Cold Zero and Hot Zero Power) are detailed that have been specially adapted to a 2D radial-azimuthal mesh of few large nodes towards an even simpler REA calculation by sNDM. Other settings, necessary at BOT (Beginning Of Transient from HZP), include fuel and coolant thermal feedbacks as well as the global conductance of a lumped thermal model. Last but not least, the special cases of a few SF found variable between BOT and EOL (End Of Launch at t = 0.05 s) are addressed by an iterative transient calculation based on their linear interpolation. This method is proven effective at the cost of accepting an irreducible discrepancy for the radial exchange rate of the ejected node, provided that a proper so-called global way of computing all SF is used. Finally, main transient results are given until EOT equilibrium (End Of Transient at t = 300 s), with various sanity checks (including a partial safety one).

CONTENTS

1. Introduction

Over the course of the last two decades, we have made multiple attempts to develop tools as light as possible for exploratory reactor physics studies. And for a few years already, we have converged to a consistent set of simple codes named KNACK (Knack of Nodal Approach to Core Kinetics) firstly introduced and demonstrated by the conference paper from which we will start (Nuttin et al., 2019). Answering our own “call for new contributions to simple approximate methods in reactor physics” made along the recent development of the sNDM diffusion method (Nuttin et al., 2023), we now propose to apply it to REA in a high converting PWR-like core. Retrieved from the previously mentioned conference paper, this core is fully heterogeneous and its calculation (described here) has required additional techniques of discretization and MC-based correction to be detailed.

Instead of using state-of-the-art codes with considerable computation costs, we decided a few years ago to focus on the simplest possible methods which could make our future analysis efforts productive within minimal times. Thanks to the limited precision needs of our planned exploratory studies on retrofitted high conversion reactors, we can indeed resort mainly to elementary diffusion theory. This robust approximation used with a coarse mesh of large homogenized nodes has already been checked to give very satisfactory results, provided that adequate associated MC models are developed for diffusion data and that some possibly necessary MC-based corrections are performed. The very first product of this approach has been the Nodal Drift Method (NDM), developed and validated around a simple CANDU LOCA benchmark (Nuttin et al., 2016). Upgraded for REA in a mini-core (Prévot et al., 2017a) and then applied to design studies of H_2O-cooled SMR cores (Prévot et al., 2017b), NDM was still found too heavy because of the discretization constraint of one node per FA (Fuel Assembly) imposed by its cartesian mesh. It has been recently generalized to sNDM (super NDM), allowing various node volumes and relying on extra MC calculations for the correction of neutron current estimations (Nuttin et al., 2023).

Validated on the KRUSTY experiment consisting like its MC model of few homogeneous zones, sNDM calls all the more for a harsher test as reactivity insertion was quite light and slow in the heat-up transient used (about 100 pcm in 600 s). Understandably, we now want to apply sNDM to a transient as quick and brutal as REA in a typical heterogeneous solid fuel core. Anticipating our future studies, we have chosen for this "crash test" one of the 600 MW_{th} D_2O/H_2O-cooled thorium-fueled Spectral Shift Control Reactor (SSCR) cores which have been previously studied by means of NDM (Nuttin et al., 2019). Starting with a convenient 2D radial-azimuthal mesh of very few nodes allowed by sNDM, the main goal here is to identify the minimal set of extra settings required for still exploitable results in our future design studies. We shall in particular pay attention to sNDM's so-called corrective Surface Factors (SF) which could be assumed constant during the KRUSTY transient but are clearly expected to evolve in the present, way more challenging, test case.

Hence this report aims at detailing the main application steps of sNDM to REA in the selected core, as a proof of practical usefulness of this method purposely developed for easy core analysis. Next sections will thus:
- sum up the main features and results of previous studies on such an innovative SSCR core (Section 2),
- propose an enhanced MCNP core design, defined at each of its HFP, CZP and HZP states (Section 3),
- upgrade specific sNDM settings related to its corrective SF and its lumped thermal model (Section 4),
- comprehensively describe the adapted, iterative calculation scheme with update of the SF (Section 5),
- present main transient results, compared to HFP, as well as some relevant sensitivities (Section 6),
- and finally conclude and give a few perspectives on the new current version of sNDM (Section 7).

2. Previous results on conversion and safety performance of SSCR

This section summarizes the main methods developed and results obtained for previously studied thorium-fueled SSCR cores (Nuttin et al., 2019) with a focus on the standard (so-called 17x17) core, which will be the only one further studied in all following sections. Similar studies have actually been performed one after another for more than ten years. First burnup calculations of modified water-cooled thorium-fueled cores, including the option of Spectral Shift Control (SSC) by H_2O additions in an initially pure D_2O coolant as originally proposed by Edlund and Rhode (1958), gave promising conversion results (Nuttin et al., 2012). Following completion of both NDM (Nuttin et al., 2016) and our C++ simulation framework SMURE (Méplan et al., 2021) which interfaces either MCNP 6 (Werner et al., 2017) or Serpent 2 (Leppänen et al., 2023) for burnup calculations, the complete set of academic methods for core design KNACK (Knack of Nodal Approach to Core Kinetics) has been conceived and applied to the design of D_2O/H_2O-cooled thorium-fueled SSC cores (Nuttin et al., 2019). In this prior study three different core lattice types, with standard 17x17 and sub-moderated 19x19 or 21x21 PWR-like FA, have been compared. Their results (burnup and conversion, then safety) are summed up here from Nuttin et al. (2019) as a necessary starting point for this report's original study.

2.1. Conversion and its usual trade-off with burnup, by SMURE

SMURE allows easy MC input generation and manages successive MC runs to compute fuel evolution under various possible user-defined constraints. Its unique multigroup flux tally feature, reducing calculation time by a minimal factor of ten with no significant discrepancy, has been used for the three core types. But let us, before giving the main results of these evolution calculations (Fig. 1), first describe our simple core design procedure.

2.1.1. Design procedure: basic choices, thermal sizing and fissile zoning

Our first design choices aim at addressing two detrimental effects on fuel utilization in SMR: neutron leakage is reduced by a ThO_2 blanket, and burnable poisons are replaced by the more flexible D_2O/H_2O SSC for reactivity management. $(Th/^{233}U)O_2$ is chosen as a convenient fuel, pretty close to its equilibrium from the start. Of course shorter-term starter fuels, e.g. based on reprocessed Pu, will be studied next. Inspired by the $(Th/^{233}U)O_2$-fueled core of the Indian Point PWR (Lung and Gremm, 1998) and based on D_2O/H_2O SSC as tested by the historical SSCR experiment (De Waegh and Storrer, 1967), our PWR-like core is made of 69 2.0-m high FA surrounded by a ThO_2 blanket and a water reflector. It is more precisely divided in four annular FA clusters, so-called zones in the following and further described in next Section by Fig. 2(a). Only the three most inner zones (numbered 1, 2 and 3) of respectively 21, 24 and 24 FA are fueled with $(Th/^{233}U)O_2$. With 28 FA, zone 4 is the radial ThO_2 blanket replacing part of neutron leakage by some extra ^{233}U production. Last but not least, the 20-cm thick axial and radial reflectors are considered as part of the primary circuit and have thus same composition as the coolant, which is 99.5 at% of D_2O at Beginning Of Cycle (BOC) and then evolves as a D_2O/H_2O mix adjusted by SSC. Such blanket and reflectors allow to keep leakage probability almost constant at about 5% in all cases.

In previous design summed up here, as well as in its updated version for this report (cf. next Section), the five radial zones have been identified with as many evolving universes for the MC transport code used (respectively Serpent and MCNP) to produce both burnup results and diffusion data zone by zone. Let us specify a few other common features of these MC models, starting with ENDF/B-VII.1 evaluated data at new standardly distributed temperatures of 300, 600 and 900 K. S(α,β) data for thermal neutron scattering are taken into account for both D in D_2O and H in H_2O. As previously used by Nuttin et al. (2012) giving all other necessary details, the external dimensions of all FA (and all fuel rods) are of the PWR N4-type with same side of 21.58 cm including 0.16 cm of water gap (and same external fuel radius of 0.41 cm). Serpent 2 and MCNP criticality calculations use either 400 active cycles of 16,000 source neutrons each (so-called "low precision" for burnup calculations by SMURE, giving a k_{eff} standard deviation of 27 pcm) or 3,200 active cycles of 128,000 neutrons each ("high precision" for fine neutron balance details, with a k_{eff} standard deviation reduced to 3 pcm). Sharing all these properties, three different core types have been studied. The first one uses standard PWR-like FA (17x17 rod positions, of which 25 filled with water stand for guide tubes) with volumic Moderation Ratio (MR) of 2.0, and will be the only one reused in this report (cf. Fig. 2). The two others are sub-moderated, with the same number of guide tubes evenly distributed among either 19x19 (MR of 1.3) or 21x21 (MR of 0.8) rod positions per FA.

Thermal sizing of each core is then performed by imposing 600 MW_{th} as its total power, which amounts to about 95 W per cm^3 of active core (zones 1-3) at BOC. Conservatively set close to standard PWR's, this average core volumic power has been checked to be acceptable together with a coolant mass flow F_{cool} set to 50 $kg.s^{-1}$ per FA (derived from PWR typical value of 100 $kg.s^{-1}$ per FA, merely halved like core height). Simple enthalpic balances of each average coolant channel allow to find back the same typical temperature rise of 40 K in all three studied core types, with a constant inlet value of 560 K (and temperature dependence of isobaric heat capacity as given at 155 bar by NIST, together with a boiling temperature of 610 K). Although heat extraction is less efficient in the two sub-moderated cases due to smaller coolant channels, it is indeed roughly compensated by the reduction of the average fuel volumic power (from about 300 $W.cm^{-3}$ in the standard case down to only 200 $W.cm^{-3}$ in the most sub-moderated one). As an extra condition imposed on our thermal sizing, the fuel volumic power in each active zone of the 17x17, 19x19 and 21x21 cases shall always remain close to its core average of about 300, 250 and 200 $W.cm^{-3}$ respectively. This has been approximately achieved by zoning fuel enrichments at BOC (with 4.0-6.0-8.0, 6.0-8.0-10.0 and 7.5-9.5-11.5 at% of ^{233}U in HN for the 17x17, 19x19 and 21x21 core's zones 1-2-3 respectively) and by checking afterwards that the radial power profile remains flat enough (over the whole cycle which is precisely described just below).

2.1.2. Common fuel cycle definition and methods, main evolution results

For simplicity sake, we have restrained on single-batch fuel cycles only. Low reactivity swings and convenient reactivity management by D_2O/H_2O SSC have indeed allowed, together with the trick of fissile zoning, to let go of any complex refueling scheme in these preliminary studies. Evolution calculations have been performed by SMURE, with Serpent 2 computing one single evolving fuel cell (and its associated multigroup flux) per zone at BOC and after each MC step for the usual update of average cross sections. For fair comparison, the same EOC (End Of Cycle) corresponding to about 1 $GW_e.y$ is set for all cores to 5 (equivalent full power) years. Consisting in the semi-continuous replacement of D_2O by H_2O in coolant (to increase its slowing-down power), SSC allows to maintain reactivity at the inevitable cost of a slight conversion loss (fewer neutrons being captured by thorium resonances). Its simulation first requires D_2O/H_2O coolant's density d_{cool} for any D_2O proportion. Pure D_2O and H_2O density values from NIST have confirmed us that the total volumic number N_{tot} of both molecules depends only on mix temperature. Evaluated to 2.38 10^{22} cm^{-3} at the average temperature of 580 K, N_{tot} simply needs to be divided by Avogadro's number and multiplied by the average molar mass (sum of the proportion-weighted molar masses of D_2O and H_2O) to give d_{cool} = 0.79 $g.cm^{-3}$ at BOC with only 0.5 at% of H_2O. The so-called BOC MC model of the core uses this value in zones 1-3, 0.83 $g.cm^{-3}$ everywhere else (at 560 K) and fuel at 900 K to give SMURE burnup calculation's run 0, at the beginning of the very first MC step. SSC simulation is based on an equivalent continuous changing rate of the H_2O proportion in coolant, supposed constant over each MC step. The same initial value of this rate, estimated beforehand for each core, is used to obtain the new coolant density values for the next MC run at the end of the first five MC steps (of 1, 4, 5, 10 and 20 days). Then, just after each new MC run of the following 40-day steps, a simple predictor-corrector algorithm uses the last two k_{eff} values to adjust the changing rate of the H_2O proportion in coolant so that reactivity remains close to zero until the end of the cycle (after 5 years of burnup at constant power). Actually all these SMURE burnup calculations have been performed during a few more years, in order to check that reactivity can no longer be maintained and decreases once coolant is eventually turned to pure H_2O. For the sake of compactness we limit the summary of our burnup results, albeit given by Fig. 1 for the three core types, to the main conversion features over the 5-y cycle.

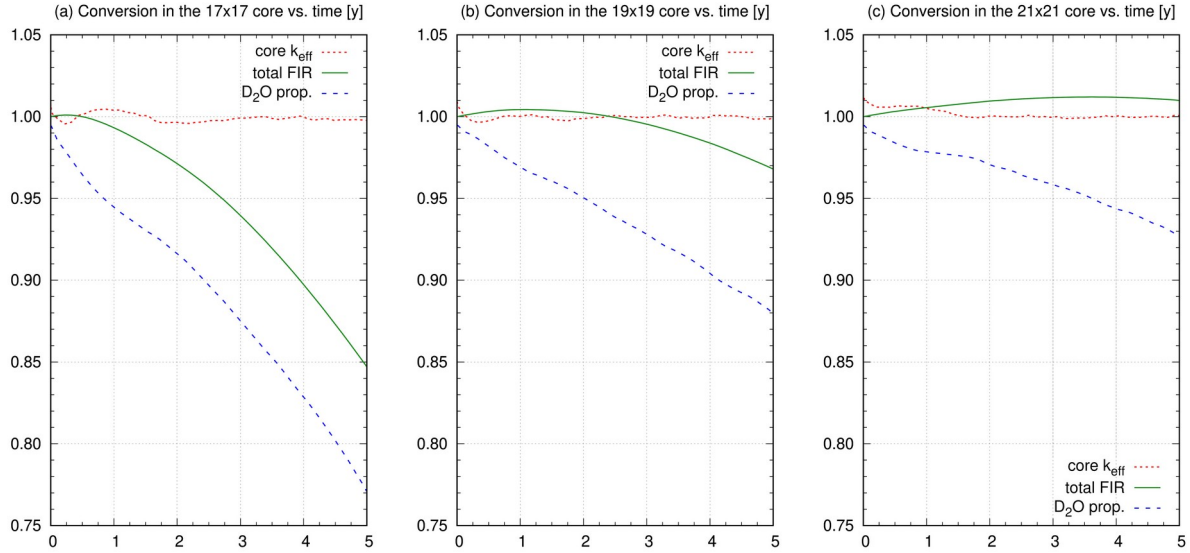

Fig. 1. Evolution of k_{eff}, Fissile Inventory Ratio (including ^{233}Pa) and D_2O proportion in coolant as key conversion results of the (a) 17x17, (b) 19x19 and (c) 21x21 cores over their common single-batch 5-y cycle as computed by Nuttin et al. (2019).

Although resulting from a very simple algorithm, k_{eff} evolutions shown by Fig. 1 are quite well-stabilized over the full 5-y cycle (with negligible impacts of their deviations from unity). The related profile of D_2O proportion in the coolant exhibits a great variation from the standard 17x17 case (where it is reduced to 77 at% at EOC) to the most sub-moderated one (where it is only reduced to 93 at% at EOC), which is all the more interesting for further design considerations as it deals with the practical question of costly D_2O recovery for next cycle. This is due to lattice sub-moderation, improving resonant capture in thorium and thus ^{233}U conversion. Let us define the FIR (Fissile Inventory Ratio), an integral indicator of conversion performance, as the ratio of core "total fissile inventory" at time t (including ^{233}U, ^{235}U and ^{233}Pa considered fully decayed into ^{233}U as if t was EOC) over its initial value (i.e. the initial ^{233}U inventory). After the same 5-y single-batch cycle, FIR amounts for the 17x17, 19x19 and 21x21 cases to 0.85, 0.97 and 1.01 respectively. Lattice sub-moderation improves conversion so well that it even makes the 21x21 core slightly breed (without ^{233}Pa decay, FIR is still 1.00 in this case).

The well-known inevitable counterpart of such an enhanced conversion is a loss of burnup (here defined per ton of HN), as analyzed by Nuttin et al. (2012) for instance. Hence, in order to complete Fig. 1's result summary, let us specify final burnup values computed by Nuttin et al. (2019) for extreme cases. Compared to 17x17's value of 48 GWd/t (with FIR of 0.85), 21x21's one is thus reduced to 31 GWd/t (with FIR of 1.01). This is due to a roughly 50 % higher HN inventory (36 tons instead of 23), imposed by the lower MR. Through sub-moderation the initial fissile inventory is even more increased, from 0.99 metric ton in the 17x17 core to 2.46 tons. Reduced to the active part of the core (i.e. excluding the blanket), the previous final burnup values are changed to about 63 and 42 GWd/t respectively. Avoiding details on various inventories (to be published in a specific paper), we only mention that the blanket shares in total energy production are about 7 and 3 % respectively. In order to give a better idea of the great conversion performance of SSCR (even in the 17x17 case), let us compare final burnup and FIR values with those of H_2O-cooled thorium-fueled full-size PWR cores as previously estimated by Nuttin et al. (2012). With 17x17 FA, such a core homogeneously loaded with same (Th/^{233}U)O_2 fuel (albeit at the lower enrichment of 3.5 at% of ^{233}U in HN) has a similar final burnup (50 GWd/t) but a much lower FIR than SSCR (0.56 instead of 0.85). With same fuel enrichment but 21x21 FA, it has likewise a final burnup (33 GWd/t) close to SSCR's one together with a way lower FIR (0.80 instead of 1.01).

2.2. Basic safety assessment on REA as design transient, by NDM

As recently summed up (2023) and initially detailed (2016) by Nuttin et al., NDM merely lets go of flux shapes and computes the number $N = \Phi V/v$ of neutrons in each of the so-called nodes subdividing the whole system (where Φ and v are respectively the one-group neutron flux and velocity, averaged over nodal volume V). Such a minimalistic approach to neutron diffusion allows to get rid of all the time-consuming continuity equations for flux and current at all interfaces. In this subsection we recall briefly how NDM has been used to compute the three SSCR cores at HFP first and then a typical REA transient from HZP for each of them (Nuttin et al., 2019), as an introduction to similar calculations to be performed by sNDM on the 17x17 core (from next Section).

2.2.1. Principles for calculation of the fully converged HFP equilibrium

For each core, the HFP state computed by NDM has provided a convenient reference that has then been used for simple REA criteria instead of more precise but less handy DNB calculations. The initial guess MC model for HFP is the same as already detailed for BOC, with coolant density set to 0.79 $g.cm^{-3}$ (580 K) in zones 1-3 and to 0.83 $g.cm^{-3}$ (560 K) in the two others (all fuel nuclide codes being set to 900 K). Each core's actual, converged HFP equilibrium is computed from this initial guess by NDM through a lumped thermal model (updating each node's average fuel and coolant temperatures, via a global fuel-to-coolant conductance G_{fuel} of a few 10^4 $W.K^{-1}$) and simple temperature dependences of all diffusion data. In this iterative process (to be reused by sNDM hence detailed below in two steps), a converged value of G (for short in the following) is obtained as well.

Starting from the BOC model for HFP and its associated G value of about 2.7 10^4 $W.K^{-1}$ (ratio of 600/69 MW as average FA power over 900-580 as temperature difference between fuel and coolant), the first step consists in the setting of all initial temperatures by NDM beforehand. In this previous study, each FA is a node for NDM and has one average temperature T_{fuel} for its fuel and another one T_{cool} for its coolant. The latter is simply forced to equilibrium as the only unknown of the two merged equations for T_{fuel} and T_{cool} time derivatives (both further detailed in subsection 4.2 for sNDM), giving a cubic equation in T_{cool} (due to the quadratic fit used for coolant's specific heat from NIST data). Once fuel and coolant temperatures are thus set for each node, diffusion data are adjusted accordingly via their temperature dependences. From this initial state, a fictive transient is computed by NDM's IRIS (Iterative Recovery of Initial Stability) simply based on the convergent $1/k_{eff}$ scaling of $\nu\Sigma_f$ values as detailed by Nuttin et al. (2016). After each of its few RK4 variable integration steps (with precursors initially reset to equilibrium), k_{eff} is estimated from all nodal rates (as the ratio of the total fission neutron production rate over the sum of the total absorption rate and the total escape rate) and used to divide all nodal $\nu\Sigma_f$ values. Once k_{eff} has finally converged to unity, the total divisor obtained is the k-eigenvalue to be applied to initial $\nu\Sigma_f$ values for perfect initial stability. In this process, neutron numbers (hence powers and nodal temperatures) converge too, together with diffusion data updated via temperature dependences. These are pre-computed for each node under the form of supposedly independent relative changes with fuel and coolant temperatures (which has been checked afterwards at our precision), from differences between the BOC model for HFP and the one for HZP (entirely at 560 K). In the latter case, Serpent's convenient Doppler preprocessing (Leppänen et al., 2023) allows to set fuel temperature precisely to 560 K. In this previous study two-group FA-homogenized diffusion data, as well as six effective delayed neutron proportions and their decay constants (one unique set for the whole core being given by the IFP method), have been directly computed by Serpent.

The second step aims at refining the G value common to all nodes through an extra detailed thermal calculation of the last obtained HFP using SMURE's BATH (Basic Approach to Thermal-Hydraulics) package, originally described by Capellan et al. (2009). For each average channel associated to one of NDM's nodes and subdivided in 20 axial levels, BATH solves energy conservation equations in its fuel, gap, cladding and coolant parts. More detailed than NDM's lumped thermal model, it is in particular based on the conducto-convective coefficient h derived from Nusselt number (itself estimated from the Dittus-Boelter correlation) and allows to recompute each FA's average fuel and coolant temperatures from its last obtained total power P (as well as its coolant mass flow of 50 $kg.s^{-1}$ per FA set at thermal sizing, among others). This way, as many (P, T_{fuel} -T_{cool}) pairs as distinct nodes (13) can be updated and, together with (0, 0) for consistency, linearly interpolated to provide an enhanced value for G of 3.8 10^4, 5.2 10^4 and 6.6 10^4 $W.K^{-1}$ for the 17x17, 19x19 and 21x21 cases respectively. Back to first step, a second HFP calculation with the new G value for each case modifies FA powers and temperatures so slightly that convergence is immediately confirmed within given precision by the following batch of BATH runs. With a maximal power of about 10 MW, each FA of zones 1-3 is checked via its BATH axial details at converged HFP to have an outlet coolant temperature at least 5 K below boiling point (of 610 K).

2.2.2. Simple 2D model for REA partially assessed by comparison to HFP

Each core's HFP equilibrium being entirely characterized, it has then been possible to use as a simple criterion for all our preliminary safety assessments (based on REA from HZP) that no FA-averaged coolant temperature should exceed its value at HFP during whole transient. This ensures, without the need for any DNB calculation, conservative margins against boiling. As the stable initial state of these transient calculations, each core's HZP has been computed in this previous study as described above for HFP, except for G which cannot be initialized at HZP low power (of only 600 W) and whose previously determined HFP value has been used instead. Here we want to complete our overview of the existing methodology to be reused by sNDM, simply by summarizing the main models and results of our previous REA calculations.

The same 2D version of NDM as previously described for HFP and HZP equilibria, with same lumped thermal model and temperature dependences of diffusion data accounting for thermal feedbacks, is used for REA. Let us specify that such a simple version has already been checked in a so-called mini-core REA benchmark to slightly overestimate nodal powers compared to a more detailed 3D version (Prévot et al., 2017a) and can thus be used here conservatively. In all the following, a so-called Control Rod (CR) refers to a PWR-like control assembly of 24 B_4C rods as described for instance by Kozlowski and Downar (2007) with the only exception in our previous study of a 90 at% enrichment of B in ^{10}B. This latter setting has been chosen by anticipating a reduced efficiency of natural boron in the hardest spectra (and in particular in the 21x21 core). Yet it has been checked afterwards to be not mandatory, and therefore natural boron will be preferred in this report's study (from next Section). The main approximation due to one single axial core level deals with the homogenization of diffusion data in any FA being partially rodded during the transient (i.e. whose CR is ejected, since neither HFP nor HZP have partially rodded FA in our studies). An ejected CR divides its FA into two sub-volumes which cannot be differentiated in 2D, making simple volume weighting (instead of a proper weighting by the product of flux and volume, in 3D) the only possible way for homogenization in our simplified model indeed.

Although REA with several CR ejected have been previously studied, we only recall here the main results for a single CR fully inserted at BOT (Beginning Of Transient) and completely ejected in 0.05 s (ejection time halved from PWR standard, like core height). Arbitrarily chosen in our previous study (contrary to this report's version adding a prior sizing of reactivity margins), the ejected FA is located at the third position on core's North-East diagonal (with central one counted as first). Let us note, as a typical result of this previous study, that only in the 17x17 case occurs the power peak after the full ejection ($3.0\ 10^5$ MW at t = 0.053 s). Due to smaller generation times (of 4.0 and 2.5 µs respectively against 7.9 µs in the 17x17 case as given by Serpent's IFP), power peaks are higher in the 19x19 and 21x21 cases (4.4 and $4.7\ 10^5$ MW) and reached about 0.005 s sooner. In all cases, the power peak consistently corresponds to the Point Of Adding Heat (POAH) when fuel temperatures start to increase. Due to its higher CR worth, the 17x17 case exhibits the highest reactivity (of about 1700 pcm, close to t = 0.05 s called End Of Launch or EOL in all the following) and the highest fuel temperatures too (with about 820 K shortly after EOL for the ejected FA). Logically, due to increased thermal inertia, fuel temperatures of other cases have been found all the lower as core lattice is tight and fuel inventory high. As regards our safety criterion, all three cases appear equivalent with the same maximal T_{cool} of 573 K reached by ejected FA (which is 5 K below its HFP value of 578 K). As a final remark on this brief account of our former safety studies, let us claim that REA can still be considered as D_2O/H_2O SSCR's most relevant design accident although its primary circuit could be flooded with H_2O in a few seconds as noticed by Lindley and Parks (2016). Such a light water ingress would have characteristics close to those of a boron dilution in a standard PWR as cleverly observed by Storrer (1967), which gives no valid reason to strip REA of its design accident status for SSCR indeed.

3. Refined core designs and their sNDM models at HFP, CZP and HZP

Starting from the previous study based on NDM and its main models which we have just summed up, this report aims at illustrating sNDM's handiness and usefulness by applying it to a similar REA calculation for the 17x17 core alone. Extending the range of possible geometries to any type of coordinates, sNDM uses here a cylindrical structured mesh with larger nodes of several FA each, for both simpler and quicker calculations. More precisely, the same five radial zones as previously defined are cylindricalized and subdivided in quarters so that transient's asymmetry can be handled by the resulting radial-azimuthal mesh of only 20 nodes for the whole core (instead of NDM's 129 nodes in previous study). Although limited since MC calculations are needed for diffusion data anyway, the price to pay for this simplification is the necessary MC-based correction of internodal and leakage currents which are only roughly estimated by Fick's law (used by sNDM as its FVM constitutive law). Each of these so-called drift rates, once multiplied by its specific pre-computed Surface Factor (SF, basically the ratio of the MC reference value over the first rough estimate by sNDM), is eventually accurate enough to contribute to reproduce almost the same neutron balance as given by the MC calculation (Nuttin et al., 2023). In this section we describe new MC models for the chosen 17x17 core, which are based on this radial-azimuthal mesh structure for easy access to both nodal diffusion data (by tally homogenization) and corrective SF (for nodal interfaces). For the latter purpose and due to its greater flexibility on geometry for current tallies, MCNP is now preferred to Serpent and used as our main MC neutron transport code (Serpent complementarily providing adjoint-weighted kinetic parameters for instance). Special effort has been made towards the completeness and consistency of our MC models of the core for its three main operating states (namely HFP, CZP and HZP) as regards the numbers and positions of inserted CR. First is described HFP, with all CR out and optimized fissile zoning. In addition to updated burnup results computed from it, we provide its diffusion data. In a second subsection, we describe CZP (checking its reactivity shutdown margin) and HZP (with its diffusion data).

3.1. For conversion and nominal thermal results at HFP (Hot Full Power)

Fig. 2(a) shows a close-up of the North-East (NE) quarter of the core as initially modelized at HFP for BOC (i.e. with T_{fuel} = 900 K and T_{cool} = 580 K in zones 1-3 and 560 K anywhere else, cf. 2.2.1) by MCNP. Unlike Serpent and its convenient Doppler preprocessing (from the same nuclear data available every 300 K), MCNP requires so-called pseudo-materials to define precise fuel temperatures (like 560 K for zone 4's fuel here) in our coming "temperature-based MCNP models" (for comparison with sNDM). As proposed by Conlin et al. (2005), used for instance by Capellan et al. (2009) and mostly justified by the variation of absorption effective integrals with the square root of absolute temperature (Lamarsh, 1966; Duderstadt and Hamilton, 1976), MCNP pseudo-material for zone 4's fuel has thus been defined as a mix with (√560 - √300)/(√600 - √300) ≈ 88.4 % of its heavy nuclei at 600 K and the remaining 11.6 % at 300 K. As regards coolant, only its density d_{cool} will have to be changed in our MCNP models. The simple linear interpolation $d_{cool} \approx 0.83 - 2.0\ 10^{-3}\ (T_{cool} - 560)$ obtained for BOC coolant from NIST data at 155 bar will be used for that purpose in all the following.

Fig. 2(b) shows the same core region after cylindricalization for sNDM. With the standard "low precision" used by burnup calculations and a k_{eff} standard deviation of 27 pcm (cf. 2.1.1), MCNP gives a cylindricalized k_{eff} (of 1.00315) compatible with cartesian one (of 1.00338). Only needed for SF with MCNP, this cylindricalized core is not used by Serpent, which gives k_{eff} values systematically 200 pcm lower (here 1.00122 at same precision). Thermal sizing is unchanged (cf. 2.1.1), with features similar to those of the boron-free SMR core designed by Alzaben et al. (2019a) and even more of B&W's mPower (as summed up for instance by Alzaben et al., 2019b). With unchanged cycle definition (cf. 2.1.2), fissile zoning has been optimized to 4.5-5.5-8.0 at% of ^{233}U in HN, so that a more balanced profile of fuel volumic power in zones 1-3 is obtained throughout the cycle while initial ^{233}U inventory of about 0.99 ton is left unchanged (with 988 kg exactly, instead of 992 kg previously).

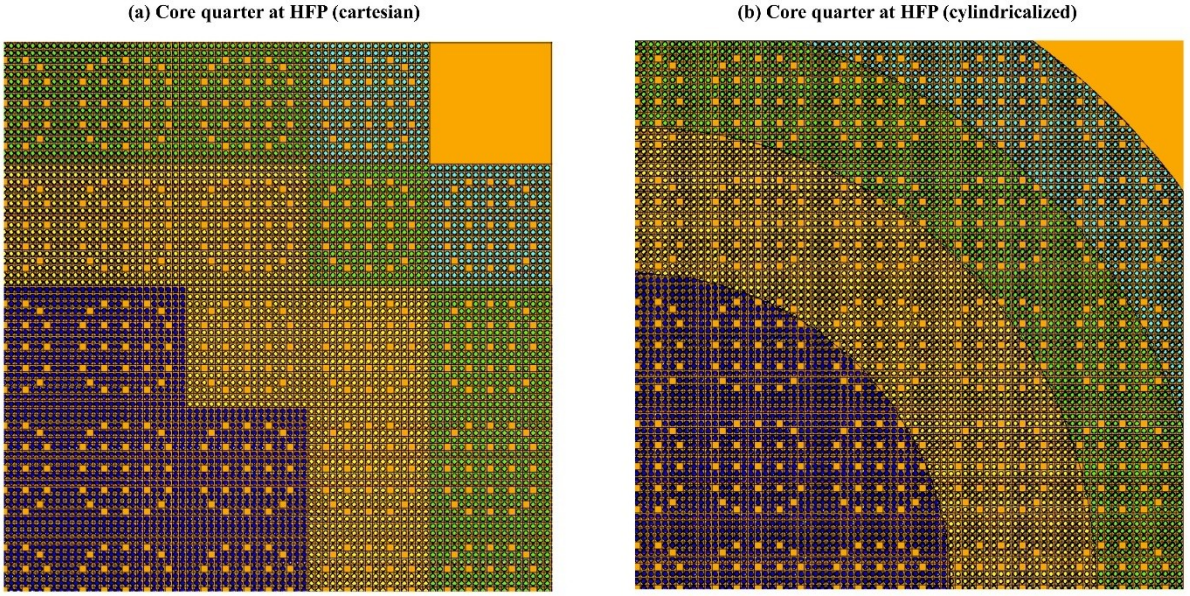

Fig. 2. Close-up of the North-East core quarter at HFP (without any Control Rod in) as geometrically modelized by MCNP, with a different color for each radial zone's fuel (violet, yellow, green and blue for zones 1-4 respectively). Water at 580 K (orange) is a material common to all zones (acting as reflector in zone 5). In the so-called cartesian model (a), zone 1 (resp. 2, 3 and 4) includes 21 (resp. 24, 24 and 28) entire FA. Its cylindricalized version for sNDM (b) conserves all zone volumes.

In comparison to burnup results previously obtained for the 17x17 core, changes are very light, in particular for FIR and D_2O proportion evolving very much like on Fig. 1(a): final FIR is still 0.85 (as the ratio of 0.84 ton over 0.99) while final D_2O proportion is slightly reduced to 75 at%. The final "fissile" inventory of 0.84 ton includes 786 kg of ^{233}U (97 kg of which are in zone 4), 20 kg of ^{233}Pa (counted as fissile for FIR) and 33 kg of ^{235}U. Final burnup of 48 GWd/t is unchanged, as well as its value of 63 GWd/t when reduced to zones 1-3. Fig. 3 concludes this cycle update by focusing on both spectral and thermal aspects of the slightly redesigned core. Normalized to total power (with typical PWR values), the neutron spectrum is shown on Fig. 3(a) to be clearly shifted towards its thermal part by H_2O additions. Fig. 3(b) shows how the radial power profile satisfactorily flattens with time, with a maximal value for zone 1 at BOC (to be specified in Section 6) and, logically, at EOC for zone 4.

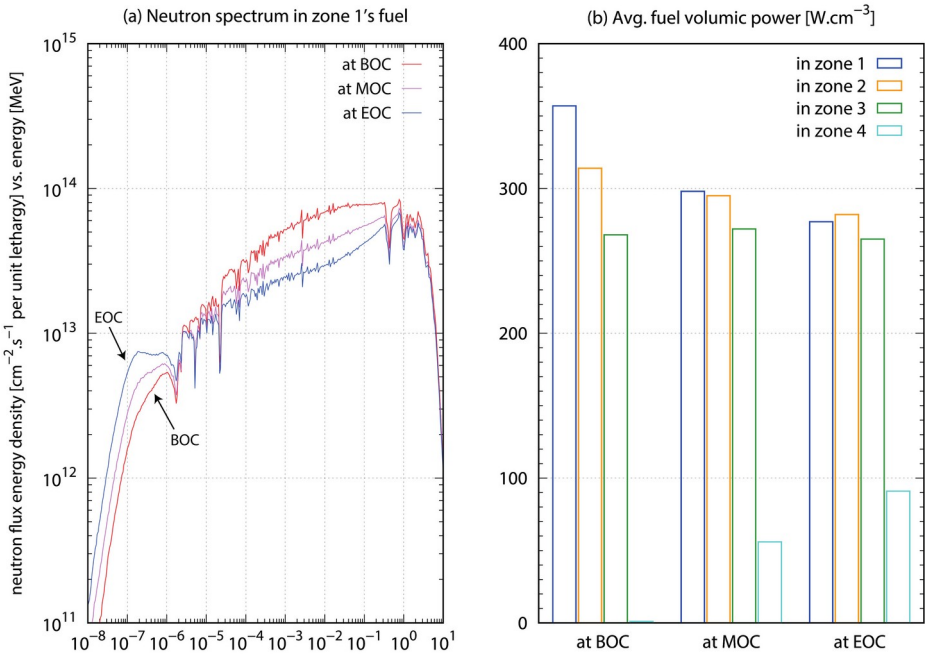

Fig. 3. Details on a few essential conversion (a) and thermal (b) features of the newly redesigned core (with 17x17 rod lattice and total power of 600 MW_{th}) at HFP (Hot Full Power). Focusing on zone 1's fuel, (a) shows the slight spectrum softening due to D_2O/H_2O SSC from BOC to EOC (with the intermediate step of MOC, Middle Of Cycle, at 2.5 y). For zones 1-4, (b) details how our optimized initial fissile zoning manages to keep acceptable fuel volumic power levels over the whole cycle.

Let us return to BOC and complete its description with all diffusion data needed by further calculations, like this of the thermal equilibrium at HFP and its average temperatures to be used as safety criteria. Table 1 gives these data for the so-called BOC model of HFP, which is nothing but the rough initial guess in the iterative calculation of the actual, converged HFP equilibrium (as already cautiously explained in 2.2.1). Contrary to previous study using two-group diffusion data with NDM, this study has switched to one-group data in full consistency with its simplifying upgrade strategy. Remarkably, the relative hardness of neutron spectrum is not the main justification of this choice, which is more directly related to sNDM letting go of flux profiles, focusing on neutron balance and thus making energy detail unnecessary. In other words, for diffusion data obtained from properly averaged MC tallies and applied to the calculation of nodal neutron numbers, one group is enough. For mere convenience, transport cross sections and velocities are obtained from Serpent (directly providing their average values in the output file). All other Table 1's data (like fission neutron production and absorption cross sections) are given by MCNP, consistently with their use for neutron balance in complement to drift rates from F1 tallies.

Table 1
Values of one-group diffusion data at HFP as homogenized from its initial MC model, either directly from Serpent 2's group constants (for transport cross section and velocity) or by ΦV-weighting over all zone's cells from MCNP tallies (for fission neutron production and absorption cross sections). Flux and volume values are given too, so that global rates (normalized to a 600 MW_{th} core power) can be obtained (core's ν being 2.506). All values are rounded accordingly to their statistical errors.

diffusion data at HFP (BOC)	**zone 1**	**zone 2**	**zone 3**	**zone 4**	**zone 5**
$\boldsymbol{\Sigma_{tr}}$ (10^{-1} cm^{-1})	2.489	2.474	2.446	2.719	2.313
v (10^{7} cm.s^{-1})	2.424	2.951	3.179	0.332	0.076
$\boldsymbol{\nu\Sigma_f}$ (10^{-2} cm^{-1})	1.029	1.095	1.397	0.011	n/a
$\boldsymbol{\Sigma_a}$ (10^{-2} cm^{-1})	0.978	0.992	1.095	0.759	0.003
Φ (10^{14} cm^{-2}.s^{-1})	8.161	6.894	4.549	1.523	0.411
V (10^{6} cm^{3})	1.933	2.209	2.209	2.578	2.946

In addition to ΦV-weighting of average cross sections, so-called "symmetry-averaging" is performed each time several nodes (subdivided in several MCNP cells) are fully equivalent by symmetry, like for instance at BOC all core quarters of a given radial zone (notwithstanding their slightly, statistically, different MC values which are simply merged). Same symmetry correction will be applied to current estimators obtained via F1 tallies. Let us add the special case of absorption cross sections, all reduced by (n,2n) cross sections (especially in water, and in fuel cells too) for the accuracy of k_{eff} values computed by sNDM as shown by Nuttin et al. (2023). Conveniently averaged over each radial zone (provided it is defined as an universe in the input), transport cross sections from Serpent (INF_TRANSPXS output values) are also preferred for their greater accuracy compared to those from MCNP (obtained as illustrated by Nuttin et al., 2016). The latter have been checked to underestimate diffusion coefficients by about 10 % for all fueled nodes, while logically the homogeneous reflector is correctly estimated this way. Adjoint-weighted kinetic parameters are given averaged over the whole core by Serpent's IFP method, including the effective delayed neutron proportions for six precursor groups (of 27, 83, 59, 129, 27 and 5 pcm, with a total of 330 ± 3 pcm) and their decay constants (of 1.25, 3.23, 10.61, 29.77, 123.5 and 634.6 10^{-2} s^{-1} respectively, giving an average value of 5.75 10^{-2} s^{-1}) used in all the following.

3.2. For safety at CZP (Cold Zero Power) and HZP (Hot Zero Power)

Special care has been addressed to the definition of core's CZP state and the estimation of the related reactivity shutdown margin or Cold Shutdown Margin (CSM). It is defined as the core reactivity with all CR fully inserted but the central one, supposed stuck in virtue of the so-called single failure criterion. With all materials at 300 K, coolant density set to 1.11 $g.cm^{-3}$ (at 155 bar from NIST) and CR as detailed by Kozlowski and Downar (2007), a satisfactory CSM of -3400 pcm (well below the required limit of -1000 pcm recalled by Alzaben et al., 2019a) is obtained with 36 CR as shown by Fig. 4(a)'s core quarter (20, 8 and 8 CR in zones 1, 2 and 3 respectively).

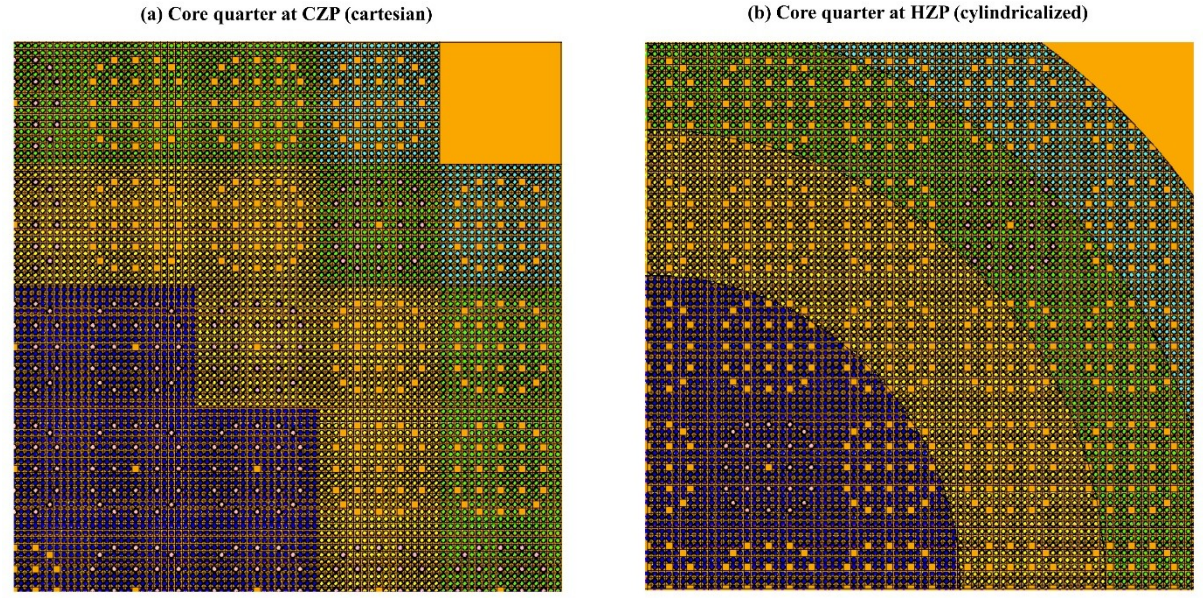

Fig. 4. Close-up of the North-East core quarter (a) at CZP in MCNP cartesian model (with 20 CR fully inserted in zone 1, 8 in zone 2 and 8 in zone 3) and (b) at HZP in MCNP cylindricalized model (with 4 CR left in zone 1 and 4 others in zone 3).

Unlike CZP model shown on Fig. 4(a) under its cartesian form, MCNP model for the HZP state (important since REA's initial state, called BOT) is given by Fig. 4(b) under the cylindricalized form which is mandatory for the calculation of the corrective SF during the transient. In addition, this latter form of Fig. 4(b) shows how each CR can still be homogenized into one single zone (provided each of these zones, like zone 3, is adequately defined). With all materials at 560 K (hence d_{cool} set to 0.83 $g.cm^{-3}$), 8 CR (two of which are visible in Fig. 4(b)'s NE core quarter) set k_{eff} both below and very close to unity as it should be at BOT (MCNP gives 0.99951 ± 3 pcm while Serpent gives 0.99653, still slightly underestimating it). As announced in this Section's beginning, the structured mesh of 20 nodes used for REA is simply made of our 5 radial zones subdivided in 4 quarters each (named NE, NW, SW and SE after the cardinal points). CR chosen to be ejected is in the second FA on NE's diagonal from the center, i.e. the most central CR shown by Fig. 4(b). Ejection will thus break symmetry and create azimuthal currents within each radial zone (two equal ones from NE to NW and to SE, themselves equally feeding SW).

Let us note that, like HFP, HZP is considered only at BOC, being the most sub-moderated and hence penalizing time of whole cycle. All other things being (almost) equal, this feature gives the lowest generation time indeed. More precisely, Λ_{eff} doubles from 6.3 µs at BOC (slightly lower than 7.9 µs in previous study, due to new fissile zoning) up to 12.2 µs (instead of 13.6 µs) at EOC. All kinetic parameters given at HFP (end of subsection 3.1) have been ckecked to remain unchanged within precision at HZP and will be used in all the following.

Table 2 gives all diffusion data at HZP necessary for the calculation of BOT (our transient's initial equilibrium), at the exception of corrective SF (to be determined next in subsection 4.1). All columns are obtained from same MC model of BOT, except the "zone 1 unrodded" one for which all four zone 1's CR are fully withdrawn (to be merely used for ejection's impact on zone 1's diffusion data). Each of these two calculations will be completed (in subsection 4.2) by two others (performed with either hotter fuel or hotter coolant) so that thermal feedbacks can be simply accounted for. Compared to HFP (cf. Table 1), homogenized cross sections and temperatures are unchanged in zones 4 and 5, while they are impacted in others by lower temperatures and inserted CR (like in zones 1 and 3). Unchanged too is the core-averaged ν value (of 2.506), which remains valid within precision for any of zones 1-3 (while zone 4's ν value is 2.415). It allows to estimate from $\nu\Sigma_f$ and Φ values all zonal powers and to check that their sum amounts to the total core power at HZP, conventionally set to 10^{-6} of HFP's.

Table 2
Values of one-group diffusion data at BOT (600 W_{th} core power), either directly from Serpent 2 (for transport cross section and velocity) or by ΦV-weighting from MCNP (for fission neutron production and absorption cross sections). While zones 4-5's data remain unchanged, zone 1's rodded data set is completed by its unrodded version (for our simple ejection model).

diffusion data at HZP (BOT)	**zone 1 rodded**	zone 1 unrodded	**zone 2**	**zone 3**	**zone 4**	**zone 5**
$\mathbf{\Sigma_{tr}}$ (10^{-1} cm^{-1})	2.556	2.546	2.525	2.506	2.719	2.313
v (10^{7} $cm.s^{-1}$)	2.442	2.205	2.769	3.116	0.332	0.076
$\mathbf{\nu\Sigma_f}$ (10^{-2} cm^{-1})	1.028	1.098	1.144	1.418	0.011	n/a
$\mathbf{\Sigma_a}$ (10^{-2} cm^{-1})	1.034	0.993	0.995	1.138	0.759	0.003
Φ (10^{8} $cm^{-2}.s^{-1}$)	6.377	n/a	7.430	4.935	1.631	0.440

4. Other sNDM settings made at BOT (Beginning Of Transient)

Thus far we have described the main features of a few D_2O/H_2O SCCR cores and new MCNP models to be used for the calculation of REA in the 17x17 version by sNDM. All necessary methods, previously used with NDM, have been recalled too, like RK4 variable integration steps in a fully explicit scheme (checked to remain stable provided the initial step is at least one order of magnitude below the typical generation time) or IRIS (cf. 2.2.1) for instance. Two key ingredients remain to be added: 1) a compact set of Surface Factors (SF) given by MCNP F1 tallies for the correction of sNDM's current estimators and 2) a simple but complete lumped thermal model.

4.1. Surface Factors (SF) as MC-based corrections of neutron currents

Before detailing our working set of SF obtained at BOT from MCNP tallies (and the associated neutron balance as exposed by Fig. 5's so-called Drift Tables), let us first recall the general principles of sNDM and then derive from these a more proper way to compute SF. Such a so-called global way has turned out to be imposed by the greater complexity of our radial-azimuthal mesh compared to the simple one used for sNDM's development and will furthermore allow us to better handle the necessary update of some SF during the transient. With only one group of precursors (and one group of neutrons) for the sake of simplicity, Eqs. (1)-(2) detail for a given node j (of average neutron velocity v_j and volume V_j) the neutron and precursor equations as solved by sNDM.

$$dN_j/dt = \text{sum over i's of } \delta_{ij} - \Sigma_a N_j v_j + (1-\beta_{eff}) \nu\Sigma_f N_j v_j + \lambda P_j \quad (1)$$

$$dP_j/dt = \beta_{eff} \nu\Sigma_f N_j v_j - \lambda P_j \quad (2)$$

$$\delta_{ij} = S_{ij} D_{ij} (\Phi_i - \Phi_j)/h_{ij} \quad (3)$$

Each term is in s^{-1} and $N_j = n_j V_j$ (resp. P_j) is the number of neutrons (resp. precursors) in node j. In sNDM and as shown by Eq. (3), the partial drift rate δ_{ij} (from neighboring node i to j) directly expresses the surface-integrated current (over the whole interface area S_{ij}) via Fick's law used as the FVM constitutive law (Nuttin et al., 2023). Fluxes are given by the numbers of neutrons ($\Phi_j = N_j v_j / V_j$). The internodal diffusion coefficient D_{ij} is computed from the two nodal P_1 transport cross sections (ΦV-weighted to give the proper average $\Sigma_{tr,ij}$ and common D_{ij}). The internodal distance h_{ij} between the two nodal positions can be expressed along any dimension. For instance in our r-θ mesh here, the azimuthal distance between two neighbor nodes in same radial zone (drift rate being of the exchange type) is the absolute difference of their nodal θ values multiplied by their common nodal radius. If neighboring node i is exterior (drift rate being then of the leakage type), h_{ij} merely reduces to the distance of j to exterior extended by the extrapolation distance $2.13\,D_j$ (while D_{ij} reduces to intrinsic D_j).

Contrary to our previous paper on sNDM which overdetailed nodal positions, taking them as average i.e. "where flux profile intercepts its average value" by means of MCNP mesh tallies (Nuttin et al., 2023), we choose in this more complex application case to define them in an easier way as constant, central positions. Such a convenient simplification will be compensated by SF, which is their main role anyway. More precisely, axial and azimuthal positions are now central (respectively located at the midplane of the single axial level and at the median angle of each azimuthal sector) while radial ones divide volume of radial zones in half. Last but not least about Eq. (3) is of course that each area S_{ij} can be multiplied by a corrective SF, so that the drift rate eventually estimated by sNDM (at any time chosen for this correction) is ideally identical (and practically much closer) to the reference value given by the related temperature-based MCNP model. This essential corrective process of sNDM, called Drift Correction (DC), is the main raison d'être of our cylindricalized MCNP models enabling calculation of all needed radial and azimuthal drift rates from adequately surface-segmented MCNP F1 tallies. In more details, an extra "FS1" tally segment card is necessary to delimit each exit surface. As it gives the total number of neutrons crossing a thus delimited surface whatever their directions, it is sufficient for the leakage type of drift rate (since no neutron comes back from exterior). The exchange type requires an extra "C1" cosine bin card to distinguish either interface side from which neutrons come. Thus the instruction "C1 0 1" gives the two oriented numbers of crossings, whose difference eventually provides the net current (and its direction via its sign).

Now we have recalled the nuts and bolts of sNDM, let us focus on the new global way of computing SF which has been the central, admittedly unanticipated, conundrum of this work. Our first attempt was made in the usual, fully local way indeed, each internodal interface having its own SF computed via its specific segmented F1 tally. But in this more complex case, it led to a few unacceptable discrepancies on reaction rates between sNDM and the associated temperature-based MCNP model (with sNDM overestimating fission neutron production rates by up to 20 % in zone 1's nodes). After several comparisons with other ways, it was eventually understood that this local way does not respect, even implicitely, all basic diffusion constraints of flux and current continuity across interfaces. Although sNDM "allows to get rid of the complex and expensive continuity conditions for flux and current at all interfaces" (Nuttin et al., 2023), it still has to implicitely respect them indeed. In the local way, SF change abruptly from one nodal interface to another that yet belongs to the same surface, which prevents current continuity and leads to discrepancies with our MC reference. Consequently the most accurate way possible for sNDM to compute SF has been checked to be based on one single average SF per full core surface that several nodal interfaces have in common. This global way will thus define and use in all the following:
- only one single axial SF, symmetry-averaged (cf. subsection 3.1) over the lower and upper horizontal surfaces of the core radially restricted by zone 5 (for axial leakage),
- one radial SF per radial interface (so five radial SF in total, the last one standing for radial leakage)
- and, by symmetry of the transient to be computed, two azimuthal SF (one for drift rates leaving the ejected NE core quarter and another for drift rates feeding the opposite SW core quarter, each one being symmetry-averaged over the two orthogonal vertical surfaces concerned that extend from core center to zone 5's external radius).

The last two types (radial and azimuthal) will have some SF partially evolving during transient and thus needing updates (as infrequently as possible for the sake of simplicity), while unique axial SF will be checked to remain constant. Beforehand let us detail the six SF values sufficient to the sNDM calculation of BOT, which needs no particular azimuthal SF value due to core symmetry in this initial state. The default value of 1.00 is thus used for all azimuthal interfaces (5 between two given quarters, so 20 in total). BOT's neutron balance is given by Fig. 5 as computed by sNDM (a) and by the reference MCNP model (b), additionally providing:
- the single axial SF of 2.46 (constant)
- and the five radial SF (from the most inner one to the most outer one) of 1.42, 0.97, 1.47, 0.76 and 0.97 (each of these values being shared by the 4 interfaces at its given radius), with second and last ones remarkably similar and close to 1.00 (due to radial flux profiles varying smoothly enough across their interfaces).

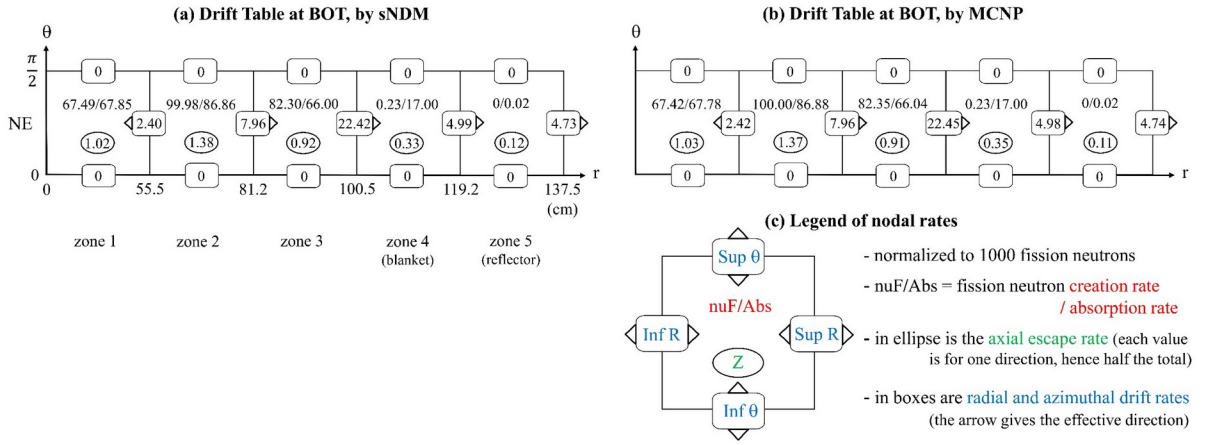

Fig. 5. Followed by their legend for one node (c), these Drift Tables (DT) give nodal reaction and drift rates obtained at BOT either from sNDM after Drift Correction and IRIS (a) or from MCNP after Criticality Correction (b). In both cases, all rates are finally normalized to a total fission neutron production rate of 1000 (s^{-1}) for the sake of readability. By symmetry all core quarters are identical at BOT: only the North-East (NE) one is shown in the r-θ plane with its five nodes, from NE1 to NE5.

Conceived as a convenient way to fully display neutron balance, the Drift Table (DT) firstly obtained for BOT is given by MCNP and Fig. 5(b). As detailed by the legend on Fig. 5(c), flux (F4) and current (F1) MCNP tallies have been exploited to fill in its boxes with normalized reaction and drift (of either the leakage or the exchange type) rates. Moreover DT has been adapted to the radial-azimuthal mesh, so that all rates remain easily readable under tabular form. As detailed for cross sections (cf. 3.1), absorption rates are all reduced by (n,2n) rates. In the case of MCNP's DT, a simple so-called Criticality Correction (CC) allows to make it perfectly balanced for fair comparison with the purely critical case of sNDM's DT at BOT. Indeed, MCNP's k_{eff} at BOT (0.99951 ± 3 pcm, cf. subsection 3.2) is close but not exactly equal to unity. CC consists thus in dividing by this k_{eff} value all nodal fission neutron production rates obtained directly from MCNP tallies, so that the new k_{eff} is forced to 1. For the sake of readability the sum of all fission neutron production rates is normalized to 1000 (s^{-1}), each of them being multiplied by the ratio of 1000 (s^{-1}) over their last sum (obtained per source neutron just after CC). This ratio, as the number of source neutrons per s, is the normalization constant which, applied to all nodal fluxes and reaction rates obtained from MCNP, gives MCNP's DT at BOT as shown by Fig. 5(b) within a precision of 1 pcm.

In the case of sNDM's DT shown by Fig. 5(a), Drift Correction (by the six initial values of SF previously given) has been followed by the equivalent of MCNP's CC for sNDM (so-called IRIS, cf. 2.2.1) to initialize BOT as a perfect equilibrium. Like for MCNP's DT, normalization of all rates to 1000 fission neutrons (produced per s in the whole core) is finally performed. Differences between MCNP's and sNDM's DT rates remain satisfactorily below a few pcm. They are caused by the new global way of computing SF that prevents fine local corrections and hence perfect agreement (as previously obtained for the propitious case used by Nuttin et al., 2023). Despite these irreducible discrepancies, it can be checked in both cases that each node (from zone 1's NE1 to reflector's NE5) is perfectly balanced within the precision of 1 pcm. For instance in NE1 as detailed by sNDM, when 67.49 fission neutrons are produced at BOT 2.40 neutrons enter from neighboring node NE2. Hence a total addition of 69.89 neutrons, exactly compensated by the total loss (67.85 by absorption and 2.04 by axial leakage).

4.2. Lumped thermal model with simple feedbacks and global conductance

A simple but complete lumped thermal model is the second key ingredient to be added. Far less tricky than SF computing, it has been slightly upgraded compared to its initial versions in our previous works. Thus it has been simplified as regards the modeling of Thermal Feedbacks (TF) via temperature dependence of diffusion data on one hand, and refined as regards the modeling of heat transfer from fuel to coolant through gas gap and cladding via one single global conductance G_{fuel} (in $W.K^{-1}$) for the whole core on the other hand.

As progressively detailed before, in subsection 3.2 (cf. Fig. 4) and in subsection 4.1 (cf. Fig. 5), each node in our sNDM model stands for a large portion of the core containing several FA (e.g. NE1, the most inner node of core quarter NE, in radial zone 1, contains the equivalent of 21/4 = 5.25 FA against 6 FA for NE2 or NE3). However, for the sake of clarity, all thermal calculations and parameters will be related to the single so-called average FA of each computed node (extensive parameters of each node being divided by its equivalent number of FA).

4.2.1. Two temperatures per node and a minimal TF model per zone

Nodal fuel and coolant temperatures T_{fuel} and T_{cool} are thus computed in K as the time-dependent solutions of the system of Eqs. (4) and (5) below, related to each node's average FA:

$$\rho_{fuel} V_{fuel} C_{fuel} dT_{fuel}/dt = P_{fuel} - G_{fuel} (T_{fuel} - T_{cool}) \quad (4)$$

$$\rho_{cool} V_{cool} C_{cool} dT_{cool}/dt = G_{fuel} (T_{fuel} - T_{cool}) - 2 F_{cool} C_{cool} (T_{cool} - T_{in}) \quad (5)$$

where:
- ρ_{fuel} (ρ_{cool}) is the fuel (resp. coolant) density in kg.m^{-3},
- V_{fuel} (V_{cool}) is the fuel (resp. coolant) volume in the node's average FA in m^3,
- C_{fuel} (C_{cool}) is the fuel (resp. coolant) heat capacity in J.kg^{-1}.K^{-1},
- P_{fuel} is the total power released in the node's average FA (and supposed to be in fuel only) in W,
- G_{fuel} is the global conductance of the fuel-to-coolant heat transfer in W.K^{-1},
- F_{cool} is the coolant mass flow through the node's average FA in kg.s^{-1}
- and T_{in} is the constant coolant inlet temperature (560 K).

Assuming that total mass remains unchanged during transient, term $\rho_{fuel} V_{fuel}$ (resp. $\rho_{cool} V_{cool}$) is kept constant, with initial density and volume of about 9.6 10^3 kg.m^{-3} and 2.79 10^{-2} m^3 (resp. 0.83 10^3 kg.m^{-3} and 5.46 10^{-2} m^3). All necessary values have been taken from NIST (2023) for the coolant and IAEA (2008) for all other materials, completed by Sobolev and Lemehov (2006) for the fuel. So C_{cool} is quadratically interpolated between 560 and 610 K (with 2.70 10^5 J.kg^{-1}.K^{-1}, -9.45 10^2 and 8.43 10^{-1} as interpolation coefficients in increasing order of degrees) while C_{fuel} is simply linearly interpolated (with 2.39 10^2 J.kg^{-1}.K^{-1} and 5.20 10^{-2} as origin ordinate and slope of its linear fit). Thus Eqs. (4)-(5), with all terms in W, are simple power balances of both fuel and coolant volumes in the node's average FA. They are coupled to Eqs. (1)-(3) via the P_{fuel} term which is equal to the nodal power (directly given by the nodal fission rate, taking 200 MeV as average energy deposited by fission) divided by the node's equivalent number of FA. In Eq. (5) a linear axial profile is supposed for the coolant temperature, which allows to replace the difference between its outlet and inlet temperatures by $2(T_{cool} - T_{in})$.

Both fuel and coolant TF are simply accounted for via temperature dependence of diffusion data, conveniently expressed by means of their Relative Changes vs. Fuel and Coolant Temperatures. Coined as RCFT (in pcm/K) and RCCT (in mk/K) respectively, these coefficients are given by Table 3 rounded accordingly to the statistical errors of the few MC calculations at their origin. These calculations have allowed us to check the relatively good independence of fuel and coolant TF within our precision. In addition to this practical independence (equivalent to negligible cross terms in interpolations), the two following approximations on NE1 (node to be ejected) have contributed to setting our precision level as given by Table 3's values. Wether NE1 is rodded or unrodded has:
- negligible effect on all other node's diffusion data (thanks to the huge size of nodes as handled by sNDM, one advantage of which being to minimize internodal neutron spectral effects)
- and negligible effect on its own TF coefficients RCFT and RCCT (^{10}B in CR having no temperature-dependent resonant absorption), hence Table 3 only gives three simple sets of such coefficients (one per core active zone).

Table 3
Relative Changes of one-group diffusion data for zones 1-3 vs. Fuel and Coolant Temperatures, coined as RCFT (in pcm/K) and RCCT (in mk/K) respectively and rounded accordingly to the statistical errors of the few MC calculations at their origin. Following ΔT_{fuel} and ΔT_{cool} changes in a zone, any of its data can be updated directly via its mere multiplication by the factor $(1 + RCFT \times 10^{-5} \times \Delta T_{fuel}) \times (1 + RCCT \times 10^{-3} \times \Delta T_{cool})$ in this simple TF model (with independent fuel and coolant effects).

	zone 1		**zone 2**		**zone 3**	
	RCFT (pcm/K fuel)	RCCT (mk/K cool.)	RCFT (pcm/K fuel)	RCCT (mk/K cool.)	RCFT (pcm/K fuel)	RCCT (mk/K cool.)
$\boldsymbol{\Sigma_{tr}}$	+0.1	-1.2	+0.2	-1.2	+0.1	-1.2
$\boldsymbol{\nu}$	+9.3	+3.6	+9.0	+3.4	+9.0	+2.9
$\boldsymbol{\nu\Sigma_f}$	-7.1	-2.2	-7.0	-2.1	-6.7	-1.9
$\boldsymbol{\Sigma_a}$	+2.9	-1.4	+3.0	-1.5	+1.2	-1.4

All Table 3's values have been computed by six MCNP full core calculations, the half of which has been needed only to check negligible effects of NE1 being rodded or not on its TF coefficients. The first of the three models with all zone 1's nodes (NE1 included) rodded stands for BOT and has been defined in subsection 3.2 (Table 2 giving its diffusion data). The two other models differ only either by fuel temperature in zones 1-3 (increased to 900 instead of 560 K) or by coolant temperature in zones 1-3 (increased to 580 instead of 560 K, i.e. with d_{cool} of 0.79 instead 0.83 $g.cm^{-3}$). Exploiting the independence of fuel and coolant TF effects (and after checking our hypotheses by versions with zone 1 fully unrodded as only difference), these three core models alone allow by the simple means of MC tallies the calculation of the few necessary values given by Table 3. The main influence of zone 4 (and its ThO_2 blanket) can be seen on zone 3's RCFT for Σ_a which is remarkably lowered compared with those of zones 1 and 2 (to +1.2 pcm/K instead of about +3.0 pcm/K).

Let us finally check how accurately we can get back Table 1's diffusion data (at HFP) from both Table 2's ones (at HZP) and our simple TF model based on Table 3's coefficients. The maximal discrepancy has been found for zone 1's $\nu\Sigma_f$ which amounts to, starting from Table 2's value at BOT for zone 1 unrodded (since we aim at fully unrodded HFP), $1.098\ 10^{-2}\ cm^{-1} \times (1\text{-}7.1\ 10^{-5} \times 340) \times (1\text{-}2.2\ 10^{-3} \times 20) \approx 1.024\ 10^{-2}\ cm^{-1}$ once reconstructed instead of $1.029\ 10^{-2}\ cm^{-1}$ as given by Table 1, hence underestimated by about 0.5 % (which is acceptable in comparison to the full variation from HZP to HFP). All other data can be likewise reconstructed, with a smaller deviation (like zone 1's Σ_a reconstructed to about $0.975\ 10^{-2}\ cm^{-1}$ instead of $0.978\ 10^{-2}\ cm^{-1}$ in Table 1). This simple TF model, entirely based on Table 3, can thus be considered sufficient for our precision needs and will be used by all our following calculations (e.g. for REA in Section 5 and for detailed HFP equilibrium in Section 6).

4.2.2. Global conductance, interpolated at HFP and adapted to HZP

Particularly during transients, so-called Pellet-Cladding Interaction (PCI) leads to changes in gap conductances which increase as powers peak and gaps shrink. Yet for the sake of simplicity, a constant global conductance G will be used as reference during the whole REA, evaluated at BOT (HZP) i.e. with the most representative value of the decisive first transient part (before EOL). Hence we will first iteratively estimate G at HFP, by following the two-step procedure already used in previous studies (and detailed in 2.2.1). This value of G at HFP will then give us access to the reference value of G at HZP, after simple corrections based on a few reasonable hypotheses about PCI during REA. Let us add that another use of G at HFP will be to still provide some kind of sensitivity to such an essential parameter lying at the heart of our thermal model, by mere comparison to reference.

Fed by Table 1's initial values for diffusion data at HFP (cf. subsection 3.1) and our TF model based on Table 3 (cf. 4.2.1), the two-step procedure detailed in 2.2.1 has been reused with same methods and settings (at the only exception of NDM replaced by sNDM). Together with the converged HFP equilibrium (which will be detailed only when needed in Section 6 for the sake of clarity), it eventually gives for G at HFP a value (unsurprisingly very close to the one obtained in our previous evaluation with NDM) of about $3.8\ 10^4\ W.K^{-1}$. With a little more details about this two-step procedure, the very first HFP equilibrium obtained after step 1 provides the power of each node's average FA (with only three values at HFP, one per active zone). In step 2, each of these powers P is used as input of a basic (BATH) subchannel calculation (with a coolant section of $2.73\ 10^{-2}\ m^2$ per FA) for the update of all nodal T_{fuel} and T_{cool} values, thus providing three updated (P, T_{fuel} - T_{cool}) pairs. Completed by (0, 0), these points give by linear interpolation a slope of about $3.8\ 10^4\ W.K^{-1}$ as the converged value of G at HFP.

Let us estimate the reference value (at HZP) of global conductance G from its value at HFP. Taking inspiration from the nice analysis of main influences on gap conductance by Alzaben et al. (2019b), we simply focus on the only significant contribution coming from conduction through the gas gap, which depends proportionally on He thermal conductivity (k_{He}) and inversely on gap width (Δr_{gap}). He conductivity dependence on temperature, from Todreas and Kazimi (2012) for instance, gives 0.23 and 0.27 $W.m^{-1}.K^{-1}$ for k_{He} respectively at HZP (560 K) and HFP (at average gap temperature of 670 K for any of zones 1-3 according to our BATH calculations). Only fuel expansion is considered for Δr_{gap} (cladding one is negligible), while fuel swelling and cracking can be neglected since core is at BOC and always near HZP. With a typical global value of a few microns only, so-called thermal jumps for an effective gap width (Todreas and Kazimi, 2012) and fuel surface roughness (Alzaben et al., 2019b) can also be neglected. From ThO_2 linear expansion coefficient of $0.9\ 10^{-5}\ K^{-1}$ (Sobolev and Lemehov, 2006), it is thus estimated that Δr_{gap} is reduced from 80 microns (at HZP) to 67 (at HFP). Consequently, a reference value of about $2.7\ 10^4\ W.K^{-1}$ is simply obtained for G at HZP by multiplying G at HFP ($3.8\ 10^4\ W.K^{-1}$) by 0.23/0.27 (k_{He} at HZP over k_{He} at HFP) and 67/80 (Δr_{gap} at HFP over Δr_{gap} at HZP, for the inverse effect of gap width).

5. Actual transient calculation, in two steps for the update of SF

Now transient calculation can be performed from the perfectly stable, neutronically equivalent to MCNP, BOT equilibrium by inserting reactivity via NE1's diffusion data (changing from rodded to unrodded during ejection until so-called EOL, End Of Launch, at t = 0.05 s). But we found quite early that a full calculation without any update of SF led to unacceptable discrepancies between sNDM's and MCNP's DT at EOT (t = 300 s). Thus one last difficulty remains to be overcome, namely the necessary update of the few fast-changing SF, as anticipated in our previous sNDM paper which identified this "as the main cause for sNDM's possible lack of accuracy in further studies" (Nuttin et al., 2023). It also added that "such variations (...) should be systematically estimated (...) from time to time, so that any SF changing too fast could possibly be updated" (and satisfactory agreement with associated temperature-based MC models could eventually be obtained). Focusing on EOL we have finally managed to implement a minimal possible SF update procedure, based in two steps. In step 1 related to ejection, changing SF are identified at EOL and linearly interpolated between BOT and EOL (subsection 5.1). In step 2, the rest of the transient (from EOL to EOT) is more easily computed, with constant SF (subsection 5.2).

5.1. First iterative step until EOL (End Of Launch)

This first step at last comes to grips with the need for SF update, particularly strong during ejection. Developed in a practical way so that it remains as simple as possible, the related method is described here in two parts. The calculation scheme itself is given in 5.1.1, where SF to be updated are first identified. These are easily provided via our temperature-based MCNP model taken at EOL, using temperatures given by sNDM after a first iteration with constant SF. But there is a catch: convergence must be obtained for all changing SF by accounting for their continuous changes over time. Fortunately, a simple linear interpolation will be shown to be sufficient. In 5.1.2 the main results obtained this way between BOT and EOL are checked against both Point Kinetics (PK) and our MCNP model, with very few discrepancies as an acceptable price to pay for such a simple update scheme.

5.1.1. SF convergence via temperature-based MCNP model

After first iteration with constant SF from BOT to EOL has been performed by sNDM, nodal fuel temperatures at EOL have been used via pseudo-materials to provide a first MCNP model of EOL (coolant temperatures still remaining very close, within tenths of degrees, to the initial value of 560 K). Then, by comparing the drift rates given by this MCNP run to sNDM's values at EOL, most of SF have been checked to remain unchanged within a few percent compared to their initial values at BOT (as given in Section 4). Only three of them have called for a significant update, each new SF value being directly obtained from the MCNP run (as the usual corrective ratio of MCNP's reference drift rate over sNDM's raw estimation from Fick's law). Thus the radial SF between zones 1 and 2 has been found equal to 2.61 (instead of 1.42 at BOT). Due to the core asymmetry newly induced by ejection (cf. Fig. 7(c) at the end of this subsection for visual help), two different types of azimuthal SF have to be distinguished: one type coined as "around NE" (related to the drift rates leaving the NE core quarter with net neutron excess during REA), and another one coined as "around SW" (related to the drift rates entering the opposite SW core quarter). And these types precisely correspond to the two other SF values which have clearly changed (to 1.92 and 1.24 respectively) compared to their initial values (set by default to 1 at symmetric BOT, when they are useless, and checked in the following to have negligible impact). Aiming at the simplest possible procedure for convergence of SF at EOL, a second iteration has then been performed by sNDM with these three changing SF linearly interpolated from BOT to EOL. Their new values obtained at EOL from our MCNP model with updated fuel temperatures have confirmed convergence within 1 %, as summed up by Table 4 which also shows how all SF are kept unchanged after EOL until EOT (cf. next subsection).

Table 4
Surface Factors (SF) identified as needing an update during transient. Their new values are obtained at EOL after the first iteration (done with all SF constant) via the associated temperature-based MCNP model, and kept unchanged since shown converged within less than 1 % after the second iteration (done with these SF linearly increased, all the other SF remaining constant during the whole transient: axial SF of 2.46, radial SF from zone 2's to zone 5's radius of 0.97, 1.47, 0.76 and 0.97).

SF values	at BOT (t = 0)	from BOT to **EOL** (t = 0.05 s)	from EOL to EOT (t = 300 s)
radial, between 1 and 2	1.42	linear increase from 1.42 to **2.61**	2.61
azimuthal, around NE	1.00	linear increase from 1.00 to **1.92**	1.92
azimuthal, around SW	1.00	linear increase from 1.00 to **1.24**	1.24

After our short description of the SF update procedure and its convergence, two clarifications remain: one about the initial value of azimuthal SF (set by default to 1), and another one about nodal fuel temperatures. Let us start with the particular case of initial azimuthal SF values, which are seemingly useless since all azimuthal drift rates equal zero at BOT. Yet another initial value than 1 for these azimuthal SF could still impact results due to their linear interpolation from BOT to EOL. This is why we have checked that taking the EOL value of each of these two azimuthal SF as its initial value (thus keeping it constant during this so-called iteration 2' or it. 2' for short) has in fact very little impact on sNDM's global results. Indeed at EOL k_{eff} is unchanged within 1 pcm (0.99086 after it. 2' instead of 0.99085 after it. 2) and so are all nodal (drift or reaction) rates, which shows that azimuthal SF values only really matter around EOL during this transient. Consequently, the default value of 1 chosen for these two SF at BOT and related iteration 2 (as detailed by Table 4) can both be kept as references without any further hesitation. Our second clarification deals with the nodal fuel temperatures obtained from our associated MCNP model, as given at EOL (after each iteration) by Table 5. Interestingly, this MC-based update of essential SF via new temperature values is similar to the update of average cross sections via new material compositions in a depletion calculation. Likewise, it is quite tolerant to a low update rate provided that the updated parameters (here SF) converge. While most sNDM fuel temperatures do not change much in Table 5, significant reductions from it. 1 to it. 2 are obtained in core quarter NE due to the important adjustment of zone 1's radial SF (towards zone 2) which tends to increase all NE's radial drift rates and thus to reduce all NE's nodal powers.

Table 5
Values of nodal fuel temperatures at EOL, as given by sNDM after each of the two iterations for SF convergence. Simply via fuel compositions using pseudo-materials is each iteration's set of fuel temperatures fed into the associated MCNP model, providing converged SF values (after it. 1, cf. Table 4) and MCNP's DT (after it. 2, cf. Fig. 7). In the radial zones 4 (blanket) and 5 (reflector), all coolant temperatures and densities (as well as fuel temperatures) remain unchanged compared to BOT.

fuel avg. temp. (K) at EOL (for MCNP)	core quarter NE		core quarter NW (or SE)		core quarter SW	
	it. 1/2	**it. 2/2**	it. 1/2	**it. 2/2**	it. 1/2	**it. 2/2**
radial zone 1	765	**732**	676	**678**	656	**659**
radial zone 2	763	**730**	694	**691**	672	**671**
radial zone 3	721	**695**	669	**666**	651	**650**

5.1.2. Accuracy checks of first transient results around EOL

Now that the full mechanism of our first sNDM step until EOL has been detailed, a few results can be analyzed as accuracy checks through the following figures (Fig. 6 to 8) with a particular emphasis on the case of zone 1's radial SF and its collateral damages on core quarter NE's neutron balance. Let us just mention beforehand that the calculation of this first part of transient (from BOT to EOL) took about 9 seconds on one single Intel i7 CPU at 2.1 GHz, hence a typical time of 3 minutes per s of transient. Such a typical time can be directly compared to our previous NDM-based REA calculation's value of about one hour per s of transient (Nuttin et al., 2019), thus exhibiting a noteworthy reduction factor of 20. The use of fewer nodes by sNDM's version (20 nodes instead of 129 FA-based nodes including reflector with NDM) gives a rough factor of 6 which is three times amplified by the mesh-induced reduction of effective exchanges between nodes. Let us add that no further computation time optimization has been performed on sNDM since its development around KRUSTY (Nuttin et al., 2023). In that case, 6 minutes have been needed per s of transient on same CPU. Using 4 nodes only (instead of 20 here), but a shorter typical integration step of 10^{-7} s (instead of 10^{-6} s), this is fully consistent with the time measured here.

In addition to a first sample of REA results over the first tenth of a second dominated by fuel thermal feedback, Fig. 6 aims at providing a comparison of step 1's iterations for a visual verification of convergence. As recalled by the legend common to Fig. 6's subfigures exhibiting the time evolution of reactivity (a), total power (b) and NE1's (or, as given by PK, average FA's) fuel temperature, step 1's first iteration (it. 1) uses constant SF (from BOT until EOL) while its second and last iteration (it. 2) linearly interpolates three of them (cf. Table 4). For the sake of comparison, Fig. 6 also indicates the results for the alternative it. 2' which interpolates only the radial SF between zones 1 and 2 (hence coined as "1 lin. SF" in the legend, with the two azimuthal SF set constant to their values at EOL). Last but not least for our verification needs, results from Point Kinetics (PK) are also provided for the related average FA, computed with same lumped thermal model and temperature coefficients estimated (to -9.5 pcm/K and -90 pcm/K for fuel and coolant respectively) from core calculations performed for Table 3. Starting from same total power of 600 W (hence an initial power of 600/69 W for its average FA) and exploiting

same value of G reconstructed at HZP (2.7 10^4 $W.K^{-1}$) than sNDM, PK uses also the same kinetic parameters as given at HFP (and conserved for HZP) together with a generation time Λ_{eff} of 6.3 µs (cf. subsection 3.2). Unlike sNDM which injects reactivity implicitely through NE1's diffusion data, PK linearly injects a total reactivity of 1100 pcm (roughly estimated from MCNP models for BOT and for its version with NE1's CR fully out) during the whole ejection period (i.e. from BOT to EOL at t = 0.05 s). Thus as shown by Fig. 6(a), contrary to sNDM's reactivity whose slope increases around mid-ejection (due to CR's enhanced efficiency around core mid-plane), PK's reactivity remains perfectly linear with its imposed slope (until about 0.04 s when fuel TF develops).

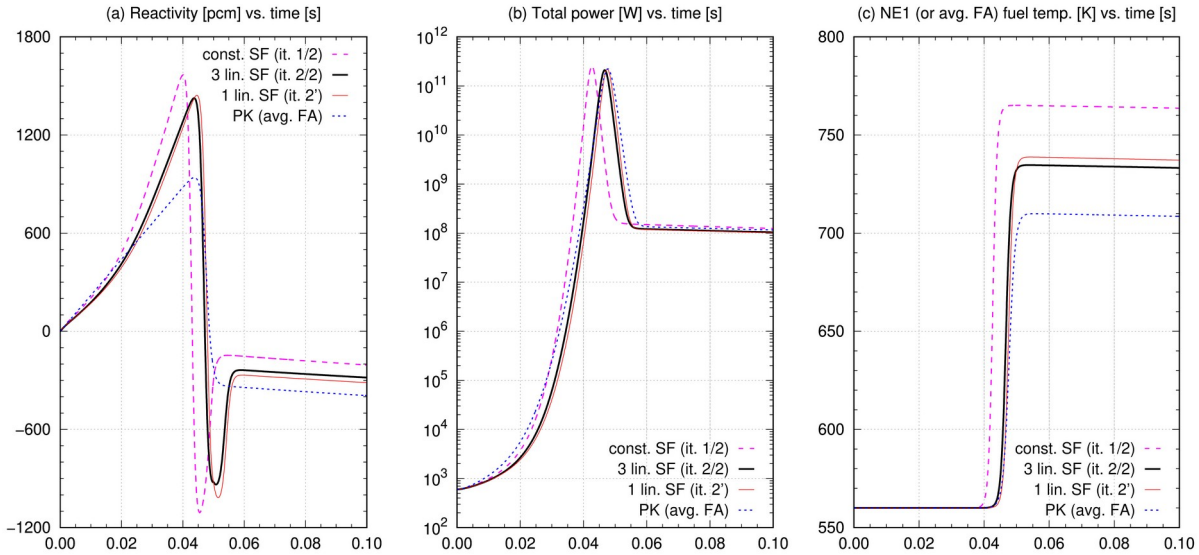

Fig. 6. Main REA results obtained by sNDM's iterations over the first tenth of a second and compared to PK on average FA (with same lumped thermal model). Despite different extreme reactivity values (reduced by point averaging of ejection and thermal feedback effects), PK results for (a) reactivity, (b) total power and (c) fuel temperature show the expected inaccuracy of first iteration (it. 1) and eventually validate it. 2/2 (linearly interpolating three SF until EOL, and close to its variant it. 2').

With a typical insertion of 1400 pcm due to the ejection of NE1's CR from HZP as depicted in 3.2 by Fig. 4(b), reactivity given by it. 2 (or 2') is clearly in much better agreement with PK than it. 1's (whose maximum is 5 ms before all others mainly because of its wrong estimation of drift rates from the very beginning). Understandably, PK's reactivity increases (and decreases after fuel thermal feedback is triggered) slowlier than sNDM's because of point averaging which attenuates both ejection and thermal feedback effects. Likewise on Fig. 6(b), while the total power peak is largely overestimated by it. 1 at 2.5 10^5 MW and 5 ms too early, it. 2's values of 2.1 10^5 MW at t = 47 ms is quite close to PK's (of 2.2 10^5 MW at t = 48 ms). Let us specify here that, since its global results are de facto correct relatively to all conservation and continuity constraints, PK can be used (albeit at core level only) as a rather trustworthy reference. Fig. 6(c) indicates a fuel temperature increase of about 170 K, which is only half that used for the calculation of Table 3's TF. Typical relative errors committed on nodal diffusion data are thus way below the maximal value of 0.5 % observed in our previous test reconstruction from HZP to HFP, which confirms that our simplified TF model (based on Table 3) is good enough for this transient. The only fuel temperature shown are NE1's, as the highest nodal value (to which NE2's is practically superimposed), and the average FA's computed by PK. Let us add by the way that NE3 is the node whose fuel temperature is the closest to PK's. For instance at t = 0.10 s when somewhat stabilized, NE3's T_{fuel} equals 696 K (against 709 K for PK's) while its average FA's power equals 1.6 MW (against 1.7 MW for PK's), which is satisfactorily consistent.

We shall now examine in detail EOL's neutron balance as given by Fig. 7, and more precisely compare sNDM's DT (directly extracted from it. 2's results at EOL) shown on Fig. 7(a) to MCNP's DT (obtained from the related temperature-based MCNP model) shown on Fig. 7(b). Like all DT in this report, these two are both normalized to the same total fission neutron production rate of 1000 (s^{-1}), giving reaction and drift rates within a precision of 1 pcm. First of all a few remarks have to be made about the changed aspect of DT. At EOL core is asymmetric as pictured by Fig. 7(c), which makes it necessary to feature all 20 nodes of our radial-azimuthal mesh under the readable tabular form of Fig. 7(a) and (b). Among them, the five nodes of the NW core quarter are by symmetry identical to the five corresponding nodes of the SE one. More precisely, the related drift and reaction rates given by sNDM are effectively identical, while their values obtained from our MCNP model are symmetry-averaged.

Let us moreover remark that each of the five azimuthal drift rates between NW and SW appears twice (θ = π and θ = -π standing for the same interface between the two core quarters). Thus on Fig. 7(a) the drift rate from NE2 (resp. to SW2) shown by a red (resp. blue dashed) arrow on Fig. 7(c) equals 0.51 (resp. 0.16) for instance. Let us add that, unlike at BOT when they are all perfectly balanced (cf. Fig. 5), nodes at EOL are clearly unbalanced and show predominant neutron losses consistently with core's sub-criticality. Each node exhibits a neutron decrease rate (due to absorption and drift outputs) higher than its increase rate (due to fission and drift inputs). For instance in sNDM's DT, when 101.94 neutrons appear in NE1 (only due to fission there), 102.14 disappear in total: 93.80 due to absorption and the rest due to (axial, radial and azimuthal) drift outputs.

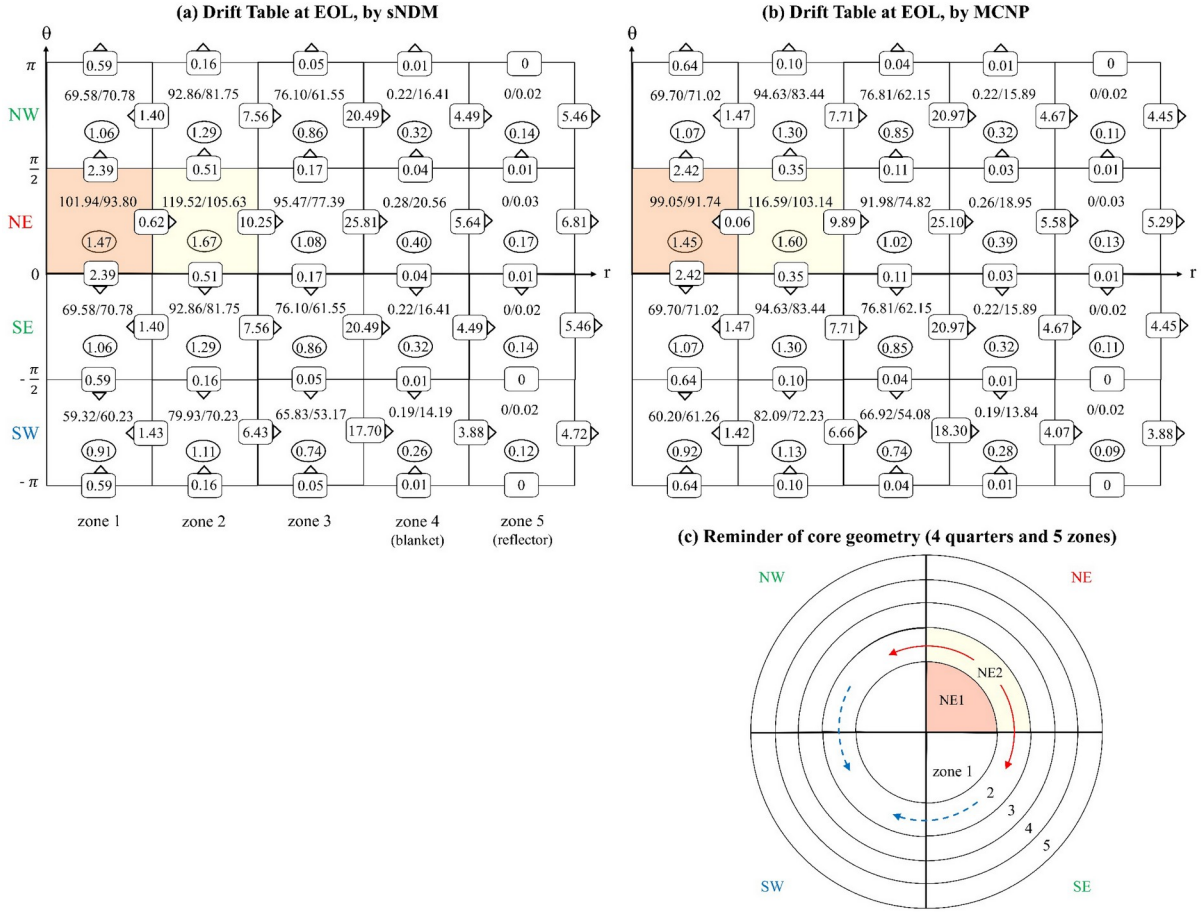

Fig. 7. Drift Tables (DT) at EOL (t = 0.05 s) according to sNDM (a) and the associated temperature-based MCNP model (b). Due to rod ejection from node NE1 (in orange), the core is now asymmetric and quarters must be detailed. To ease reading, the corresponding 2D geometry is given (c) with red (blue dashed) arrows illustrating for zone 2 the equal azimuthal currents leaving NE (reaching SW). The highest fission neutron production rate is obtained in NE1's neighbor node NE2 (in yellow).

Although NE2's fission neutron production rate is easily noticed in both DT to be much higher than NE1's, it should be recalled that each node contains the equivalent of 6 FA in zone 2 (24 FA being equally shared between core quarters) instead of only 5.25 in zone 1 (filled with 21 FA). By accounting for these respective FA numbers (both nodes sharing the same core-averaged ν value), NE2's average FA is thus found to have a power only about 3 % higher than NE1's one, which explains why these nodes have close temperatures. All nodal reaction rates are similar within a few percent between sNDM's DT and its MCNP-based version used as reference. This is not the case for some of the radial drift rates, especially in the NE core quarter, which seem overestimated by sNDM compared to MCNP. One such nodal drift rate, particularly poorly reconstituted at EOL by sNDM, is the radial drift rate between NE1 and NE2 (of -0.62, i.e. leaving NE1, according to sNDM against 0.06 according to MCNP). Although the agreement on this rate is very good at fully symmetric BOT (cf. Fig. 5), it progressively deteriorates until EOL whose strong asymmetry makes it impossible for the related global SF to reproduce such a local effect. Despite this flaw, we can guarantee that present sNDM version is by far the best methodological compromise we have found hitherto. As for all the other radial drift rates exhibiting some minor discrepancies with MCNP (mainly in NE), they are mere consequences of this original flaw

propagated from NE1 down to radial zone 5. Indeed radial drift rates of all nodes either in the NE core quarter or in radial zone 5 (reflector) appear slightly overestimated in sNDM's DT compared to MCNP's. And so do the related nodal fluxes, with increasing overestimations of 1.5, 3.0, 4.1, 8.5 and 28.6 % checked along the NE core quarter from NE1 to NE5 (where the absorption is very low and extra neutrons from NE1 logically accumulate). Similarly in the other quarters, flux overestimations of about 3 and 22 % build up from BOT until EOL in zones 4 and 5 respectively. Such a cumulative effect of overestimated fluxes (and hence drift rates) culminates at EOL when sNDM inaccuracies are the worse. Thereafter they have been checked to vanish, as all SF remain constant due to unchanged geometry after ejection. Tolerated for the sake of proper SF calculations, the annoying discrepancy on NE1's radial drift rate has thus limited consequences in both space and time.

Let us complete this analysis at EOL by a few more global comparisons. According to sNDM and Fig. 6(a) k_{eff} at EOL is about 0.991, against 0.997 as given by our MCNP model. This sNDM (resp. MCNP) k_{eff} value can be precisely reconstituted by Fig. 7, as the ratio of 1000 neutrons produced by fission over the sum of 956.24 (resp. 955.15) absorbed and 52.99 (resp. 48.17) escaped. And with a bit more details, the main part of k_{eff} discrepancy is easily attributed to the same previous problem of NE1's radial drift rate leading to overestimated radial escape rates. Indeed sNDM (resp. MCNP) total escape rate includes a radial one of 22.45 (resp. 18.07 only), giving the main part of the 600 pcm missed by sNDM at EOL. Another set of global comparisons, extended over the first tenth of a second, is given by Fig. 8 which shows how NE1's flawed radial drift rate (so-called NE1/SupR in the following) evolves around EOL and compares it to two others (namely NE5/SupR and NE1/Supθ).

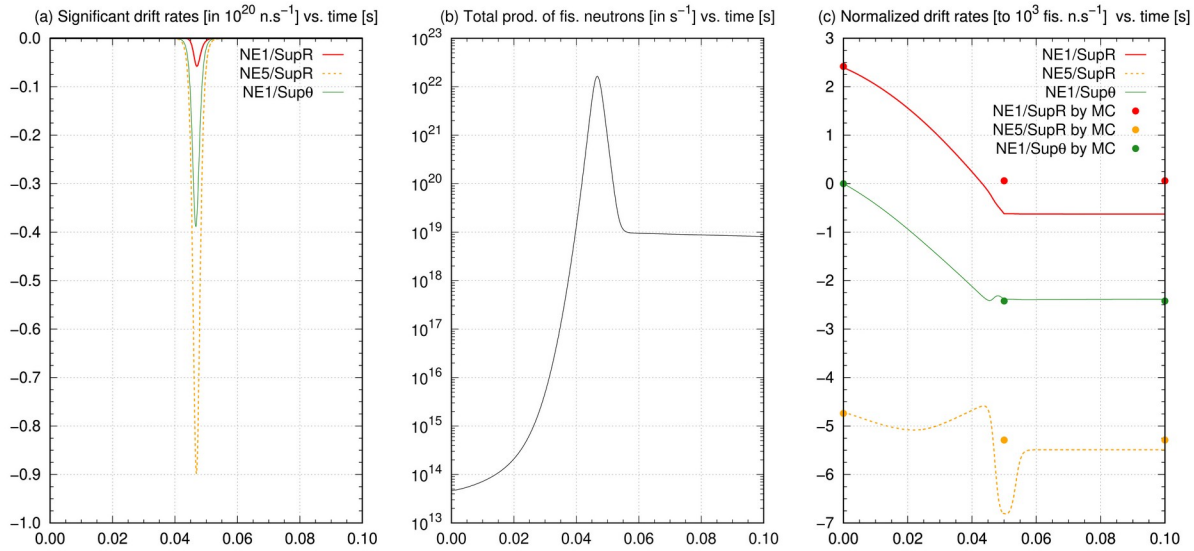

Fig. 8. Time evolution, over the first tenth of a second, of the SupR drift rates of NE1 and NE5 nodes together with the Supθ drift rate of NE1. Although NE1/SupR drift rate is initially positive (NE1 receiving a net positive neutron current from NE2), significant values are all negative (a). For better detail and comparison to reference values from a few MC static calculations, the total production of fission neutrons (b) is used to normalize these drift rates to 10^3 fission neutrons per s at all times (c).

By scrutinizing these drift rates of three different types, Fig. 8 aims at giving a better idea of the time evolution of their respective accuracy as computed by sNDM. Starting from the sNDM values shown by Fig. 8(a), this is realized by normalizing them to the same total fission neutron production rate (reduced to 10^3 s^{-1}) at all times for the sake of readability via its original values shown by Fig. 8(b), and by comparing them as pictured on Fig. 8(c) to the corresponding ponctual values computed at BOT, EOL and t = 0.10 s (round colored dots) by the related temperature-based MCNP models. Inspired by traffic lights (with red standing for constantly flawed, orange for temporarily inaccurate and green for regularly accurate), Fig. 8(c)'s color code depicts NE1/SupR's case as the worse since its sNDM value is clearly different from MCNP's at EOL and remains so until t = 0.10 s at least. NE5/SupR's case is intermediary (showing at EOL the same type of inaccuracy which tends to vanish thereafter though) while NE1/Supθ is a good example of the majority case with satisfactory accuracy at any time. All this confirms the particular status of the NE1/NE2 interface in our sNDM calculation. Last but not least, it confirms also that no other core states than EOL is really needed for the update of SF. Indeed an extra state for SF update, such as the mid-launch one for instance (at t = 0.025 s), would cure neither the inevitable flaw of NE1/SupR nor its few temporary side effects (while requiring additional MCNP calculations together with axial averaging).

5.2. Final direct step until EOT (End Of Transient)

The second and last step of the transient calculation by sNDM is much easier than the troublesome first one, as all SF have been checked to remain constant over it. This latter feature explains that the nodal fuel and coolant temperatures obtained by sNDM at EOT (final equilibrium at t = 300 s) are directly converged. These values are given for all heated zones by Table 6 and are the basic ingredients to be injected in our MCNP model eventually providing sNDM's and MCNP's DT at EOT as detailed by Fig. 9. In addition to pseudo-materials, let us recall that our MCNP model only uses the linear dependence of coolant density with temperature (cf. subsection 3.1).

Table 6
Values of nodal fuel and coolant temperatures, as given by sNDM at EOT. In the temperature-based MCNP model for EOT, fuel temperatures are taken into account via pseudo-materials and coolant temperatures via adapted densities in related cells.

fuel and coolant temp. (K) at EOT	core quarter NE		core quarter NW (or SE)		core quarter SW	
	fuel	coolant	fuel	coolant	fuel	coolant
radial zone 1	658	565.0	627	563.4	617	562.9
radial zone 2	656	564.9	634	563.8	623	563.2
radial zone 3	636	563.9	620	563.1	612	562.6

So based on Table 6's temperatures, MCNP's DT at EOT shown by Fig. 9(b) is obtained and allows us to finish assessing our full transient calculation by comparing it with sNDM's DT shown by Fig. 9(a) for the same final equilibrium. Sure enough the only remaining discrepancy is located at the interface between NE1 and NE2, with sNDM's and MCNP's values for NE1's radial drift rate at EOT (-0.62 and 0.05 respectively, from the point of view of NE1's balance as usual) very close to those obtained at EOL (cf. Fig. 7). All the other drift and reaction rates are, between sNDM and our MCNP reference, in much better agreement at EOT than at EOL. As a state, EOT has been chosen at a time advanced enough that the core is practically back to full equilibrium according to sNDM. Thus sNDM's DT, directly obtained as shown by Fig. 9(a), allows to reconstitute a k_{eff} value of 1.00000 (i.e. unity within 1 pcm) as the ratio of 1000 neutrons produced by fission over the sum of 951.44 absorbed and 48.56 escaped (30.48 axially and 18.08 radially). In the case of MCNP's DT, like at BOT (cf. Fig. 5), Criticality Correction and the renormalization of the total fission neutron production rate to 1000 (s^{-1}) have been necessary to bring MCNP's k_{eff} value (of 0.99947 ± 3 pcm) back to unity for the sake of comparison. Reading Fig. 9(b) we can thus count, for 1000 fission neutrons produced, 951.58 absorptions and 48.42 escapes (30.34 axial and 18.08 radial). The agreement of these global rates at EOT with sNDM's is very satisfactory, confirming (in particular via their common radial escape rate) that the few discrepancies analyzed at EOL were both local and temporary.

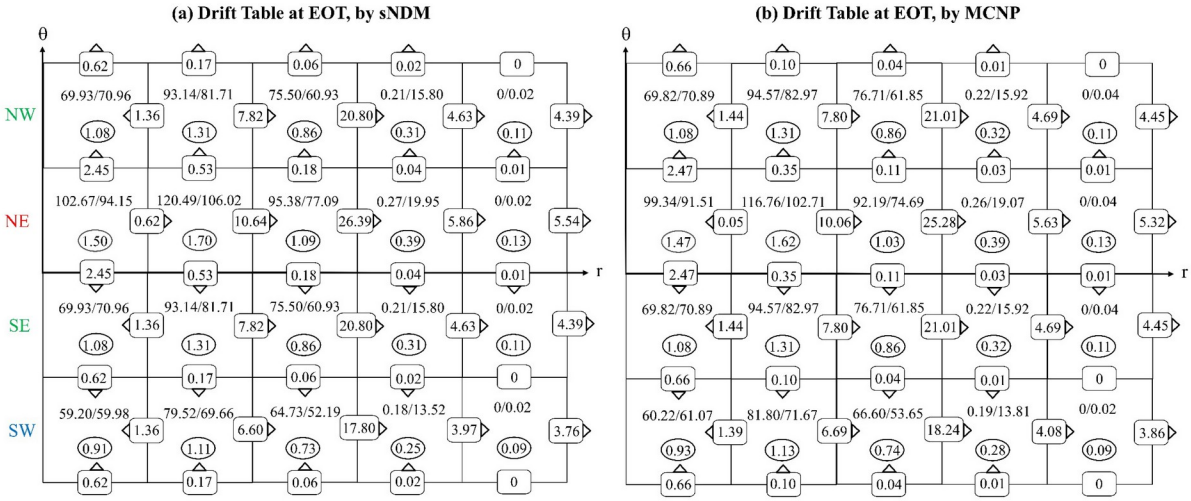

Fig. 9. Drift Tables (DT) at EOT (t = 300 s) according to sNDM (a) and the associated temperature-based MCNP model (b). With a common k_{eff} value checked to be perfectly equal to unity at this final equilibrium, these DT show a very satisfactory agreement (at the only inevitable exception of the radial drift rate between NE1 and NE2, explained in previous subsection).

6. Partial safety assessment with HFP temperatures as simple criteria

At this point we may consider that our main objective to demonstrate sNDM's operational efficiency on such a demanding transient as REA has been reached. Notwithstanding the short-lived flaw at ejected node (which we have fully analyzed as an acceptable side-effect of the proper way of SF calculation), sNDM has been shown to be both light (with few pre-computed data) and accurate enough for our research needs. In this section we aim at discussing further transient results, most specifically towards safety assessment. Thus subsection 6.1 gives a few remaining important results and analyzes them in both terms of sensitivity to G value and of comparison to PK. Then subsection 6.2, as a final complement, focuses on the HFP equilibrium and deduces from this a few partial and preliminary conclusions about safety mainly for the sake of completeness.

6.1. Main transient results and relevant sensitivities

With a final equilibrium value of about 100 MW_{th} as shown by Fig. 6(b), core's total power has been confirmed to remain during most of this transient well below its nominal value of 600 MW_{th} at HFP. As a result the global conductance G at HZP (obtained in subsection 4.2) can be regarded as its best representative value for our REA calculation. Nevertheless, among the additional transient results displayed by Fig. 10, some have been obtained with G at HFP as an alternative (so-called "alt. G") value to provide a first element of (thermal) sensitivity. To a lesser extent (limited to reactivity), PK results have also been added as a second element of sensitivity (to spatial treatment of kinetics) and for specific indications (on global thermal feedbacks) as well.

As shown on Fig. 10(a) by so-called "PK's coolant" reactivity (integrated coolant temperature coefficient), the minimum shared by all versions around t = 0.5 s is mainly due to coolant TF with a complement of a few tens of pcm only from the already heated fuel. Reactivity changes much less rapidly on this larger time range of a few seconds, which explains that all results are closer to each other than on previous Fig. 6(a). Let us add that PK's coolant reactivity consistently shares the same evolution (with the same maximum around t = 1.0 s) than coolant temperatures on Fig. 10(c), to be detailed in the following together with the corresponding average FA powers of Fig. 10(b). PK's fuel reactivity is not represented since out of scale: it first drops down to about -1400 pcm at t = 56 ms, then slowly increases back up to reach -700 pcm at t = 5.0 s (when PK's reactivity of 100 pcm can be decomposed as 1100 pcm inserted, reduced by -700 and -300 pcm from fuel and coolant TF respectively).

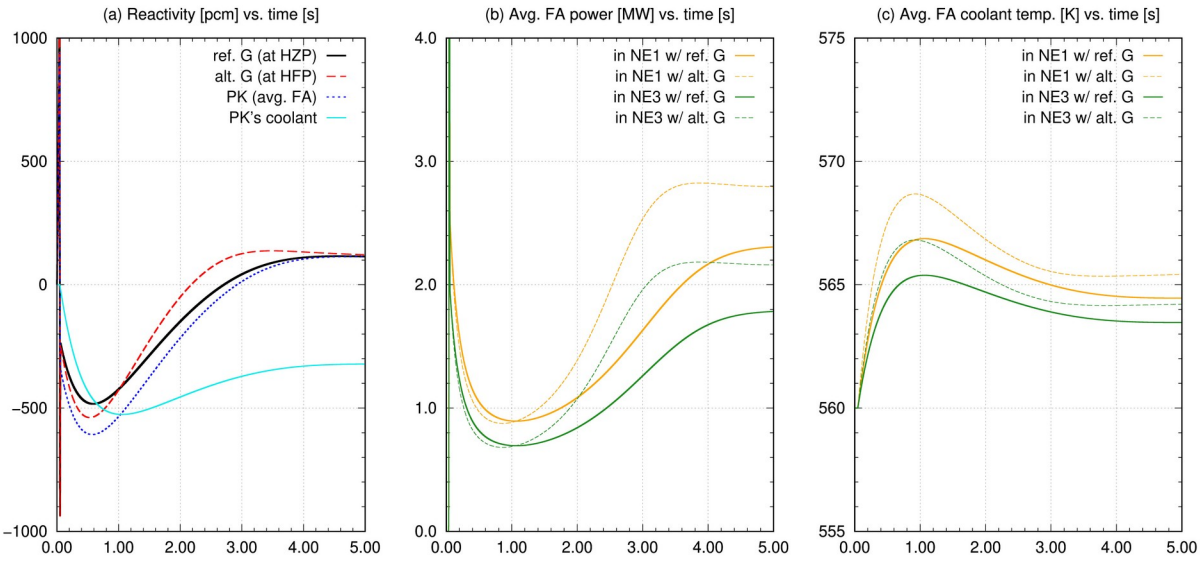

Fig. 10. Main REA results obtained by sNDM over the first five seconds, with sensitivity to the global conductance value G and emphasis on coolant temperature. Using G at HFP (instead of reference value at HZP) gives lower fuel temperatures (by typically 10 K), hence higher (a) reactivity and (b) average FA powers. Consistently, coolant temperatures (c) are higher too.

Let us now focus on average FA powers and coolant temperatures, given by Fig. 10(b) and (c) respectively, for nodes NE1 and NE3 only. As previously observed over the first tenth of a second, NE2 still shows such results (including fuel temperature) very close to NE1's and therefore is not represented. Similarly, NE3 has its average FA's results very close to those of both NW2 (or its symmetric node SE2) and PK (not represented either).

As previously noticed for fuel (in 5.1.2), maximal coolant temperature rises are less than half the 20 K increase used for our TF model (based on Table 3), which appears detailed enough. This is all the more true as fuel and coolant temperature rises are pretty well time-separated. Furthermore, it should be noted that PK provides a few convenient consistency checks via the comparison of its results to NE3's (by sNDM), for instance at remarkable times t = 0.5 s (reactivity minimum) and 5.0 s (reactivity maximum, close to final equilibrium). Thus at t = 0.5 s NE3's FA power is about 0.8 MW against 0.9 MW for PK's, while NE3's T_{fuel} (T_{cool}) is 683 K (564.4 K) against 694 K (564.8 K) for PK's. Likewise at t = 5.0 s NE3's FA power is 1.8 MW against 2.0 MW for PK's, while NE3's T_{fuel} (T_{cool}) is 628 K (563.5 K) against 630 K (563.6 K) for PK's. At this same time t = 5.0 s but using the higher alternative G (of 3.8 10^4 $W.K^{-1}$ at HFP), both a lower T_{fuel} (of 620 K instead of 628 K) and a higher T_{cool} (of 564.2 K instead of 563.5 K) are logically obtained for NE3. Given the typical (PK's) fuel and coolant TF (of about -10 pcm/K and -90 pcm/K respectively), these temperature differences (of -8 K and +0.7 K respectively) induce a higher reactivity (by about 17 pcm) and hence a higher FA power (of about 2.2 MW at t = 5.0 s, instead of 1.8 MW with reference G). Let us complete this subsection by describing how nodal fuel temperatures evolve over the same time range: from times close to EOL, they all decrease steadily due to heat extraction by coolant. Thus for instance (with reference G) NE1's T_{fuel} decreases from 735 K at its peak time t = 54 ms (just after EOL) down to 648 K at t = 5.0 s, with a very slow re-increase up to 658 K at EOT. This last slight increase is simply due to the remaining reactivity (of about 100 pcm at t = 5.0 s, as previously detailed) which is then progressively reduced to zero (and converted in slightly higher powers and temperatures) until EOT.

6.2. Detailed HFP equilibrium and final safety analysis

In order to bring some first insight into the safety level of the studied core against REA (as its design accident), let us estimate NE1's (maximal) fuel enthalpy deposit (albeit only from a nodal, i.e. averaged, point of view). It is directly obtained by integrating the fuel heat capacity (linearly interpolated in temperature , cf. 4.2.1) between 560 K (at BOT) and 735 K (maximal NE1's T_{fuel} value), which gives 11 cal/g. Compared to a typical local limit of 230 cal/g (Alzaben et al., 2019b), this value is so low that we are tempted to regard it as conclusive although it is only average. But anyway sNDM, by its principles, lets go of all results more detailed than nodal ones. Thus we have no choice but to use the HFP equilibrium as a conservative reference for maximal coolant temperatures, while sticking to the nodal temperatures provided by our sNDM calculation of the transient. In other words, the simple criterion chosen for preliminary safety analysis needs is that no nodal (FA-averaged) coolant temperature should exceed its corresponding HFP value. Indeed the latter sets an acceptable limit, indirectly validated by our conversative core design which implicitely account for DNB margins. Hence this subsection is mainly dedicated to the calculation of the HFP state, exploited for its nodal coolant temperatures as basic safety indicators.

Actually, calculation of HFP equilibrium has already been described (in 4.2.2, together with the estimation of G) and follows the same two-step procedure as initially detailed for NDM (in Section 2): nodal powers obtained by sNDM (step 1) are fed into the simplified subchannel code BATH for both the update of nodal temperatures and the estimation of G by linear interpolation (step 2, checked to be definitely converged). In its first two columns, Table 7 gives zone by zone the nodal FA powers and their related fuel volumic power values (remarkably close to those obtained from the so-called BOC model of HFP, shown by Fig. 3 in subsection 3.1). These same values, input into BATH, provide refined nodal fuel and coolant temperatures (in Table 7's double columns 3 and 4).

Table 7
Main thermal results given by sNDM's lumped thermal model at HFP (with global conductance G of 3.8 10^4 $W.K^{-1}$ and core at BOC), compared to the more detailed BATH code used to compute the average channel related to each zone with same fuel volumic power. Inlet coolant temperature is set to 560 K and boiling temperature is 610 K (for BOC coolant at 155 bar).

	avg. FA power (MW)	fuel volumic power ($W.cm^{-3}$)	avg. fuel temp. (K)		avg. coolant temp. (K)		out. coolant temp. (K)
	by sNDM	by sNDM	sNDM	BATH	sNDM	BATH	by BATH
radial zone 1	9.99	358	838	849	578.6	583.8	602.7
radial zone 2	8.94	320	809	811	576.8	581.4	598.8
radial zone 3	7.71	276	775	770	574.6	578.5	594.0

Due to interpolation, sNDM's temperatures logically give for each zone the same G of about 3.8 10^4 $W.K^{-1}$ (as the ratio of FA power over T_{fuel}-T_{cool}) while BATH gives three slightly different values (increasing from slightly less than 3.8 10^4 $W.K^{-1}$ for zone 1 up to 4.0 10^4 $W.K^{-1}$ for zone 3). It explains why sNDM's T_{fuel} is a bit lower

than BATH's in zone 1 (and vice versa in zone 3). For all zones sNDM's T_{cool} is systematically underestimated in comparison to BATH (accounting for a more detailed heat transfer to coolant), which gives a good idea of the relative accuracy of our simplified thermal model. Table 7's last column gives the outlet coolant temperature for each zone (more precisely the average value of the last axial level among the 20 ones used by BATH), allowing us to check that the core's thermal sizing is satisfactory. Let us specify, as a sensitivity test, that zone 1's outlet coolant temperature has been checked to exceed the boiling temperature (of 610 K) by only 1 K with a coolant mass flow reduced to 40 $kg.s^{-1}$ (instead of 50 $kg.s^{-1}$) per FA. Now Table 7 has been fully detailed, let us finally confront its HFP coolant temperatures with their corresponding maximal values predicted by sNDM during the transient. For the sake of compactness and clarity, we focus on nodes NE1 and NE3 (though it has been checked that all other nodes have their coolant temperatures well below their HFP values during REA). Let us recall that NE2 is thermally close enough to NE1 (just as both NW2 and its symmetric node SE2 are to NE3), so that NE1 and NE3 are representative of the five most heated nodes during REA. As can be seen on Fig. 10(c) the highest value for NE1's T_{cool} maximum is 568.7 K, obtained at t = 0.92 s by sNDM (with alternative G). By about 10 K, this transient value is lower than even the lowest NE1's HFP T_{cool} (of 578.6 K, according to Table 7 and sNDM). Likewise (from sNDM with alternative G) NE3's T_{cool} maximum is 566.8 K at same time, well below its lowest HFP value of 574.6 K. And it has been checked that so do all other nodes, which fully satisfies our simple safety criterion that "no nodal coolant temperature should exceed its HFP value". Of course, since nodal temperatures are averaged indicators, such a safety check is only partial and calls for further thermal details. It is nonetheless a good and very easily obtained hint that our thermal sizing is acceptable. Not only from a nominal point of view (over the full cycle) but from a transient one too, allowing to avoid DNB crisis during REA.

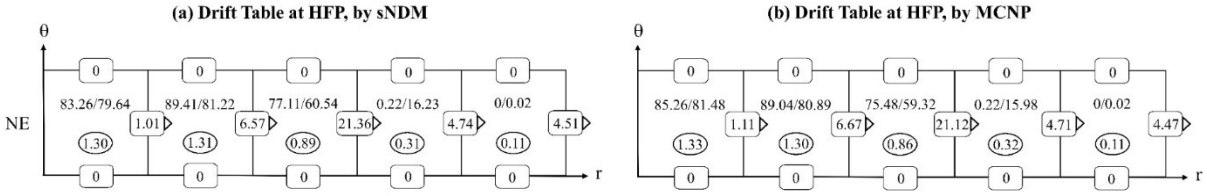

Fig. 11. Drift Tables (DT) at HFP according to sNDM (a) and to the associated temperature-based MCNP model (b), given as an ultimate check. Like at BOT (but without any CR in), all core quarters are identical and only NE is represented.

Fig. 11(a)'s DT as obtained at HFP by sNDM is a natural complement to its thermal results of Table 7. Provided it is duly normalized by the node's number of FA, each fission neutron creation rate is thus easily checked to be consistent with the related FA power given by Table 7. For instance, the ratio of NE2's fission neutron creation rate over NE3's (89.41/77.11) from Fig. 11(a) is logically identical to the ratio of NE2's FA power over NE3's (8.94/7.71) from Table 7. By comparison, MCNP's DT at HFP shown by Fig. 11(b) can be considered as a final check of sNDM's satisfactory accuracy. Like previously for the BOT, EOL and EOT transient states, it has been simply obtained by using sNDM's temperatures (given in Table 7) in our temperature-based MCNP model thus applied to HFP. Compared to our so-called BOC model of HFP (with 900 K as uniform T_{fuel} and a k_{eff} of about 1.003, cf. subsection 3.1), this refined MCNP model has fuel temperatures lower by about 100 K and thus a k_{eff} higher by about 1000 pcm (in virtue of core's fuel temperature coefficient of about -10 pcm/K). Consequently, for the sake of direct comparison with sNDM's DT like at EOT, MCNP's DT at HFP has been brought back to equilibrium by CC and renormalization of all rates to the usual total fission neutron production rate of 1000 (s^{-1}) which is here equivalent to 250 per core quarter since HFP is fully symmetric. Hence both Fig. 11's DT are fully balanced, with k_{eff} values exactly equal to unity (like BOT as detailed by Fig. 5's DT for instance). These can be decomposed as follows for sNDM (MCNP): for 250 neutrons produced by fission in NE, 237.65 (237.69) are absorbed and 12.35 (12.31) escape with 7.84 as common axial escape rate.

Let us specify that, like for BOT and EOT, HFP's DT are locally balanced too (each node being balanced within a precision of 1 pcm). Residual flux overestimations (as analyzed in 5.1.2) explain that all rates remain slightly overestimated by sNDM in the most outer radial zones, while it is exactly the other way around for zone 2 and zone 1 especially (with a maximal discrepancy for NE1's radial drift rate, underestimated by about 10 %). Thus this ultimate check strengthens our confidence in the reasonable accuracy of the sNDM diffusion method, even when applied to such a complex and harsh transient test case. And as a cherry on the cake, it also validates our basic two-step method for HFP equilibrium calculation (detailed and used at several occasions in this report).

7. Conclusions and perspectives

This work has been principally concerned with the application of our sNDM diffusion method to the demanding calculation of REA in an innovative PWR-like SMR core. Such a core has been the subject of previous studies whose main settings and results have been summed up in Section 2, with regard to both conversion performance (over a whole 5-y single-batch cycle) and safety level (during REA via simple comparison to HFP equilibrium). Carefully designed with conservative thermal sizing and optimized fissile zoning, all core versions (with various fuel lattices) of this D_2O/H_2O-cooled thorium-fueled SSCR core have shown great potential for high conversion. Moreover, they have offered the opportunity to give a first description of our basic methods for REA calculation as well as for HFP equilibrium calculation. Needed for quick safety assessment, the latter is based on a two-step procedure feeding nodal powers into a more detailed thermal code (than the simple lumped thermal model used) and eventually comes up with the tandem of a converged solution and its related global conductance G (properly accounting for heat extraction by the coolant). Among the three cores studied, only the 17x17 version has been selected as a test case for switching from NDM (our first standard diffusion method) to sNDM (conceived to use even larger nodes by means of a FVM approach based on Fick's law). In the latter method, correction of current estimations is necessary and performed via so-called Surface Factors (SF), obtained from MCNP F1 tallies and anticipated to be variable in complex transients such as REA in a PWR-like core. All needed MCNP models, for all core states (including HFP for safety assessment, CZP for shutdown margin and HZP as REA's initial state), have been thoroughly described in Section 3. Subdivided into 5 radial zones (by adapted cylindricalization) and 4 quarters (for a radial-azimuthal mesh of only 20 nodes in total), each MCNP model of the core has been used to produce one-group diffusion data (by standard homogenization over each node). Carrying over these methods and models to an actual REA calculation by sNDM, we have developed in Section 4 a proper (so-called global) way of computing SF which has finally allowed us to implicitely respect the basic constraints of flux and current continuity across nodal interfaces. In addition to this essential upgrade, we have refined the global conductance of our thermal model by estimating its more representative value at HZP from our prior HFP calculation.

All these preparative steps have given rise to a much clearer understanding of how to finally perform the actual REA calculation with sNDM, as detailed in Section 5 which gives a comprehensive account of the first iterative step dedicated to SF update until the end of CR ejection (EOL). In this delicate first step, the continuous update of only one among eight used SF (the radial one between central zones 1 and 2, highly impacted by CR ejection from node NE1) has been found to be mandatory. Simple linear interpolation between its BOT and EOL values (both obtained from our corresponding temperature-based MCNP models) has been proven to be sufficient. So it has been demonstrated that, even in such a fast-changing first step, sNDM can get by with minimized updates of its basic parameters and still provide sufficiently accurate results. Admittedly, one particular drift rate (radially between the ejected node NE1 and its neighbor NE2) has exhibited a flaw around EOL. Identified on sNDM's neutron balance (Drift Table or DT) at EOL compared to MCNP's, it has however been shown to remain local and temporary with limited consequences and has been accepted as the lesser of two evils (other one being the local way of computing SF which has been checked in our preparatory works to lead to incorrect reaction rates). Thus, despite this tolerated flaw of the poorly reconstituted drift rate NE1/SupR (and its few collateral damages on core quarter NE), sNDM has proven until final equilibrium (EOT) a sufficiently accurate method for full core calculations dedicated to exploratory design studies. This strong and promising conclusion has been reinforced in Section 6 by additional transient results showing great consistency and satisfactory accuracy, in particular as regards HFP equilibrium. By mere comparison of coolant temperatures during REA with their HFP values, this core's safety has been assessed: admittedly only partially (since without any local DNB details), yet consistently with our previous results (obtained by a more detailed NDM calculation of similar REA in same core).

Hence we can definitely conclude that the current sNDM version, applicable to full core calculations while only needing very few MC-based diffusion data and corrective factors, is the best methodological compromise we have found so far. Representative of so-called conventional nodal methods, sNDM estimates currents "in terms of differences in node-averaged fluxes for adjacent nodes, with empirically adjusted coupling coefficients" as defined by Stacey (2001). MCNP provides such an empirical (or rather numerical) adjustment via SF obtained from F1 tallies, together with a secure way to identify the changing ones. Even more than we have claimed for its previous version (Nuttin et al., 2023), sNDM offers "interesting pedagogical applications (illustrating basic notions like MC tallies, diffusion approximation and neutron balance)" due to its increased simplicity. Using SF in so close connection with temperature-based MC models of a core is probably the quintessential recipe for its easiest analysis. Also noteworthy are the gains offered on computation time, mainly due to the reduced number of nodes allowed by azimuthal mesh. For all these reasons, we now dare to present sNDM as a DIY toolkit for simple core calculations and we hope that some readers will efficiently apply it to their own studies.

In terms of perspectives, it could be tempting to preferentially go back to further developments. For instance, it may appear interesting to implement 3D nodalization as well as two-group neutron equations and diffusion data. Yet in line with our pragmatic approach that "better is the enemy of good enough" we believe that the extra cost of complexity and computation time would not be justified by the accuracy gain, for we have already witnessed this with NDM before. Moreover, as previously stated, two-group diffusion would not enhance accuracy, due to "sNDM letting go of flux profiles, focusing on neutron balance and thus making energy detail unnecessary". Of course, exterior models like the lumped thermal one could still be improved (with more detailed heat exchanges or fuel and coolant cross terms taken into account in the temperature dependence of diffusion data). But again, our main concern remains to preserve sNDM's maximized "accuracy vs. complexity" ratio. As a consequence, we rather plan to apply sNDM to the study of SSCR concept evolutions. More precisely, our priority objective is to devise an alternative way of reactivity management keeping coolant composition unchanged (with its BOC proportions of D_2O and H_2O). Getting rid of the efficient SSC based on H_2O addition (possibly too expensive due to D_2O regeneration costs), a solution could be to use reactivity reserve provided by rotating control drums in the reflector (with their absorbing parts oriented towards the core at BOC). As well for static as for transient calculations of such a core, sNDM's azimuthal mesh option developed in this report could be very useful.

Acknowledgements

First of all, we would like to thank the Slow Science initiative for its inspiring conception of a research report as the final outcome of a patient artisanal work. For our interesting exchanges, many thanks to Naoyuki Takaki (Tokyo City University) and Armando Dominguez (Canadian Nuclear Laboratories) met at IAEA's Consultancy Meeting on Thorium-Based Water-Cooled Reactor Concepts held last May in Vienna.

References

Alzaben, Y. et al., 2019a. Core neutronics and safety characteristics of a boron-free core for Small Modular Reactors. Ann. Nucl. Energy 132, 70-81.

Alzaben, Y. et al., 2019b. Analysis of a control rod ejection accident in a boron-free small modular reactor with coupled neutronics/thermal-hydraulics code. Ann. Nucl. Energy 134, 114-124.

Capellan, N. et al., 2009. 3D coupling of MC neutronics and thermal-hydraulics calculations as a simulation tool for innovative reactor concepts. Proc. Int. Conf. GLOBAL 2009.

Conlin, J.L., Brown, F.B., Mosteller, R.D., 2005. Temperature corrections in MCNP for calculating the Doppler defect. Report LA-UR-05-6225, Los Alamos National Laboratory.

De Waegh, F., 1967. BR3/Vulcain core performance: theoretical and experimental aspects. Proc. Symp. on heavy-water power reactors held by IAEA in Vienna.

Duderstadt, J.J., Hamilton, L.J., 1976. Nuclear Reactor Analysis, John Wiley & Sons.

Edlund, M.C., Rhode, G.K., 1958. Spectral Shift Control. Nucleonics 16, 80-81.

IAEA, 2008. Thermophysical Properties of Materials For Nuclear Engineering: A Tutorial and Collection of Data, <www-pub.iaea.org/MTCD/publications/PDF/IAEA-THPH_web.pdf>.

Kozlowski, T., Downar, T., 2007. PWR MOX/UO_2 Core Transient Benchmark. Final Report NEA-6048, OECD Nuclear Energy Agency.

Lamarsh, J.R., 1966. Introduction to Nuclear Reactor Theory, Addison-Wesley.

Leppänen, J. et al., 2023. Online User Manual for Serpent 2, <serpent.vtt.fi/mediawiki>.

Lindley, B.A., Parks, G.T., 2016. The Spectral Shift Control Reactor as an option for much improved uranium utilisation in single-batch SMRs, Nucl. Eng. Design 309, 75-83.

Lung, M., Gremm, O., 1998. Perspectives of the thorium fuel cycle, Nucl. Eng. Design 180, 133-146.

Méplan, O. et al., 2021. SMURE: a Serpent-MCNP Utility for Reactor Evolution, Computer Program Services of OECD Nuclear Energy Agency and <lpsc.in2p3.fr/MURE/html/SMURE/UserGuide/UserGuide.html>.

NIST, 2023. Thermophysical Properties of Fluid Systems, <webbook.nist.gov/chemistry/fluid>.

Nuttin, A. et al., 2012. Comparative analysis of high conversion achievable in thorium-fueled slightly modified CANDU and PWR reactors. Ann. Nucl. Energy 40, 171-189.

Nuttin, A. et al., 2016. Validation of the minimalistic Nodal Drift Method for spatial kinetics on a simple CANDU LOCA benchmark. Ann. Nucl. Energy 88, 135-150.

Nuttin, A. et al., 2019. Study of D_2O/H_2O-cooled thorium-fueled PWR-like SMR cores using the KNACK toolbox: conversion and safety assessment. Proc. Int. Conf. ICAPP 2019, <hal.in2p3.fr/hal-03782798>.

Nuttin, A. et al., 2023. Development and dual validation on a transient inspired by KRUSTY of the sNDM diffusion method for easy, MC-based, core analysis. Ann. Nucl. Energy 180, 109469.

Prévot, P., Nuttin, A. et al., 2017a. Enhancements to the Nodal Drift Method for a Rod Ejection Accident in a PWR-like mini-core with lumped thermal model. Ann. Nucl. Energy 101, 128-138.

Prévot, P., Nuttin, A. et al., 2017b. Preliminary design studies by a complete academic simulation toolbox of a water-cooled thorium-fueled Small Modular Reactor core. Proc. Int. Conf. GLOBAL 2017.

Sobolev, V., Lemehov, S., 2006. Modelling heat capacity, thermal expansion and thermal conductivity of dioxide components of inert matrix fuel. Journal of Nuclear Materials 352, 300-308.

Stacey, W.M., 2001. Nuclear Reactor Physics, John Wiley & Sons.

Storrer, J., 1967. BR3/Vulcain nuclear power station: construction and operational experience. Proc. Symp. on heavy-water power reactors held by IAEA in Vienna.

Todreas, N.E., Kazimi, M.S., 2012. Nuclear Systems Volume 1: Thermal Hydraulic Fundamentals, CRC Press.

Werner, C.J. et al., 2017. MCNP User's Manual, Code Version 6.2. Report LA-UR-17-29981, Los Alamos National Laboratory.